Mon. Not. R. Astron. Soc. **387,** 158–172 (2008) doi:10.1111/j.1365-2966.2008.13104.x

Radiation from early black holes – I. Effects on the neutral intergalactic medium

E. Ripamonti,[1,2]★ M. Mapelli[3] and S. Zaroubi[2]

[1]*Dipartimento di Fisica, Università di Milano-Bicocca, Piazza della Scienza 3, I-20123 Milano, Italy*
[2]*Kapteyn Astronomical Institute, University of Groningen, Postbus 800, NL-9700AV Groningen, the Netherlands*
[3]*Institute for Theoretical Physics, University of Zürich, Winterthurerstrasse 190, CH-8057 Zürich, Switzerland*

Accepted 2008 February 12. Received 2008 February 12; in original form 2007 October 17

ABSTRACT

In the pre-reionization Universe, the regions of the intergalactic medium (IGM) which are far from luminous sources are the last to undergo reionization. Until then, they should be scarcely affected by stellar radiation; instead, the X-ray emission from an early black hole (BH) population can have much larger influence. We investigate the effects of such emission, looking at a number of BH model populations (differing for the cosmological density evolution of BHs, the BH properties, and the spectral energy distribution of the BH emission). We find that BH radiation can easily heat the IGM to 10^3–10^4 K, while achieving partial ionization. The most interesting consequence of this heating is that BHs are expected to induce a 21-cm signal ($\delta T_{\rm b} \sim 20$–30 mK at $z \lesssim 12$) which should be observable with forthcoming experiments (e.g. LOFAR). We also find that at $z \lesssim 10$ BH emission strongly increases the critical mass separating star-forming and non-star-forming haloes.

Key words: black hole physics – galaxies: formation – intergalactic medium – cosmology: theory – diffuse radiation.

1 INTRODUCTION

The Sloan Digital Sky Survey[1] (SDSS) has unveiled the existence of quasars at redshift $z \gtrsim 6$ (Becker et al. 2001; Djorgovski et al. 2001; Fan et al. 2001, 2002, 2003; White et al. 2003). This indicates that supermassive black holes (SMBHs) with a mass of $10^{9-10}\,{\rm M}_\odot$ had already formed when the Universe was less than 1 Gyr old (Fan et al. 2001, 2003).

The processes which lead to the formation of such huge black holes (BHs) already in the early stages of the life of the Universe are very uncertain. A possible scenario is that SMBHs were built up starting from a seed intermediate-mass BH (IMBH, i.e. a BH with mass of 20–$10^5\,{\rm M}_\odot$), which increased its mass by accreting gas and/or by merging with other IMBHs.

In particular, if first stars are very massive ($>260\,{\rm M}_\odot$) their fate is to directly collapse into BHs, nearly without losing mass (Heger & Woosley 2002). This can produce a population of IMBHs, which are expected to efficiently accrete gas in the high-density primordial Universe and eventually to coalesce with other BHs (Volonteri, Haardt & Madau 2002, 2003; Islam, Taylor & Silk 2003, 2004; Volonteri & Perna 2005; Volonteri & Rees 2005, 2006). Furthermore, the accretion of these IMBHs might be enhanced also during galaxy mergers, which tend to drive gas into the inner regions of the host galaxy (Madau et al. 2004). However, recent simulations by Pelupessy, Di Matteo & Ciardi (2007) suggest that the accretion history of such seed IMBHs can hardly account for the SMBHs of the SDSS.

On the other hand, seed BHs can be produced also by the direct collapse of dense, low angular momentum gas (Haehnelt & Rees 1993; Umemura, Loeb & Turner 1993; Loeb & Rasio 1994; Eisenstein & Loeb 1995; Bromm & Loeb 2003), driven by turbulence (Eisenstein & Loeb 1995) or gravitational instabilities (Koushiappas, Bullock & Dekel 2004; Begelman, Volonteri & Rees 2006, hereafter BVR06; Lodato & Natarajan 2006). In particular, the so-called 'bars within bars' mechanism (Shlosman, Frank & Begelman 1989, 1990) implies that bars, which form in self-gravitating clouds under some assumptions, can transport angular momentum outwards on a dynamical time-scale via gravitational and hydrodynamical torques, allowing the radius to shrink. This shrinking produces greater instability and the process cascades. BVR06 show that this process leads to the formation of a 'quasi-star', which rapidly collapses into a $\sim 20\,{\rm M}_\odot$ BH at the centre of the halo. The BH should encounter very rapid growth due to efficient gas accretion.

This allows the formation of seed BHs with mass $\lesssim 10^6\,{\rm M}_\odot$ (BVR06; Lodato & Natarajan 2006, 2007), depending on the initial parameters (e.g. the temperature of the gas and the spin parameter of the parent halo).

If such seed BHs formed at high redshift ($z \sim 10$–30), they likely played a crucial role in the early Universe. Previous

★E-mail: ripa@astro.rug.nl
[1] http://www.sdss.org/

studies (Machacek, Bryan & Abel 2003; Madau et al. 2004; Ricotti & Ostriker 2004, hereafter RO04; Ricotti, Ostriker & Gnedin 2005, and references therein) showed that IMBHs accreting as miniquasars could be important sources of partial, early reionization. The efficiency of miniquasars in reionizing the high-redshift Universe is especially due to the hardness of their spectra, which extend up to the X-ray band.

For this reason, miniquasars are also indicated as sources of the X-ray background, and their density can be strongly constrained by the level of the unresolved fraction of this background (RO04; Dijkstra, Haiman & Loeb 2004; Ricotti et al. 2005; Salvaterra, Haardt & Ferrara 2005; Volonteri, Salvaterra & Haardt 2006; Salvaterra, Haardt & Volonteri 2007).

Finally, miniquasars can also heat the intergalactic medium (IGM; see e.g. Nusser 2005; Zaroubi et al. 2007, hereafter Z07+; Thomas & Zaroubi 2008), influencing a plethora of processes (the 21-cm line emission/absorption, the formation of the first structures, etc.).

In this paper, we analyse all the main effects that primordial miniquasars can produce on the neutral IGM, that is, on the regions of the Universe outside the ionized regions produced by the first BHs and stars. This is done by means of semi-analytical models combined with hydro-dynamical simulations. We consider all the most-significant models for miniquasar formation, density evolution and spectra. Whereas previous studies mostly focused on single aspects, our aim is to give a global description, as complete as possible, of the role played by IMBHs in the early Universe.

In particular, in Section 2 we will present an estimate of the radiation background produced by primordial BHs at high redshift. We will then discuss its effects on the IGM evolution, and in particular on the cosmic microwave background (CMB) spectra and on the 21-cm emission (Section 3). In Section 4, we will discuss whether the radiation background can delay structure formation. In Section 5, we will discuss the relevance of our findings in light of previous results. Finally, our results will be summarized in Section 6.

We adopt the best-fitting cosmological parameters after the three-year *WMAP* results (Spergel et al. 2007), that is, $\Omega_{\rm b} = 0.042$, $\Omega_{\rm M} = 0.24$, $\Omega_{\rm DM} \equiv \Omega_{\rm M} - \Omega_{\rm b} = 0.198$, $\Omega_\Lambda = 0.76$, $h = 0.73$, $H_0 = 100\,h$ km s^{-1} Mpc^{-1}.

2 ENERGY INJECTION INTO THE NEUTRAL IGM

2.1 The total energy input

First of all, we develop a formalism for estimating the total energy input of BHs into the neutral IGM at a given redshift, starting from basic properties of the BH population, taken from semi-analytic models (see next Section), such as the BH mass density $\rho_{\rm BH}$ at redshift z, the average BH mass $\langle M_{\rm BH}\rangle$ at redshift z, and the duty cycle y of single BHs.

We start from considering that the mean free path of a photon of energy E emitted at redshift z is:

$$\lambda(E, z) = [n_{\rm B}(z)\sigma(E)]^{-1}, \tag{1}$$

where $n_{\rm B}(z) = n_{\rm B}(0)(1+z)^3$ is the cosmological baryon number density at redshift z [$n_{\rm B}(0) \simeq 2.5 \times 10^{-7}$ cm^{-3}; Spergel et al. 2007], and $\sigma(E)$ is the photo-ionization cross-section per baryon of the cosmological mixture of H and He, which is approximately

$$\sigma(E) = \begin{cases} 0.75\sigma_{\rm H}(E) & 13.6 \leqslant E \leqslant 25\,{\rm eV} \\ \sigma_{250}\,[E/(250\,{\rm eV})]^{-2.65} & 25 \leqslant E \leqslant 250\,{\rm eV} \\ \sigma_{250}\,[E/(250\,{\rm eV})]^{-3.3} & 250\,{\rm eV} \leqslant E, \end{cases} \tag{2}$$

where $\sigma_{\rm H}(E)$ is the photo-ionization cross-section of hydrogen (see equation 2.4 of Osterbrock 1989), and $\sigma_{250} \simeq 3.2 \times 10^{-21}$ cm^2 is the cross-section for 250 eV photons (see Zdziarski & Svensson 1989 for further details on the cross-section at $E > 25$ eV). In this paper, we will neglect the absorption of photons with $E < 13.6$ eV. It is important to note that the above cross-section is appropriate only for a neutral gas. Since the IGM close to luminous sources is mostly ionized (and the ionized fraction is not zero even in mostly neutral regions), equation (1) might lead to an underestimation of λ, but this effect is important only in the last phases of reionization.

On the other hand, the average distance between 'active' BHs is

$$d = \left[\frac{\rho_{\rm BH}(z)\,y}{\mathcal{C}\,\langle M_{\rm BH}\rangle(z)}\right]^{-1/3}, \tag{3}$$

where $\mathcal{C}$ accounts for the clustering of BHs.[2]

The comparison of λ and d shows that for photons of sufficiently high energy the mean free path can easily exceed d. For instance, the mean free path of a 500 eV photon emitted at $z = 20$ is about 9 comoving Mpc ($\sim d$ in typical models), but at the same redshift a 1-keV photon typically propagates for $\sim$90 comoving Mpc. Since BHs are believed to emit a significant fraction of their luminosities at such energies, they will build up a roughly uniform background radiation field.

The BH emissivity can be estimated by assuming that during active phases of accretion, each primordial BH produces radiation at a fraction η of the Eddington luminosity [$L_{\rm Edd} \simeq 1.3 \times 10^{38}$ erg s^{-1} $(M_{\rm BH}/{\rm M}_\odot)$], and that their average spectrum at redshift z is described by some function $F(E, z)$. The proper emissivity is then

$$j(E, z) = \mathcal{L}\,\frac{F(E, z)}{\int F(E', z)\,{\rm d}E'}\,\rho_{{\rm BH},\odot}(z)\,\left(\frac{\eta}{0.1}\right)\,y\,(1+z)^3, \tag{4}$$

where $\mathcal{L} \simeq 4.4 \times 10^{-37}$ erg s^{-1} cm^{-3} M$_\odot^{-1}$ is a normalization constant[3], and $\rho_{\rm BH,}(z)$ is the BH density at redshift z, expressed in solar masses per cubic comoving Mpc.

The mean specific intensity of the radiation background at the observed energy E, as seen by an observer at redshift z, is then (cf. equation 2 of Haardt & Madau 1996):

$$J(E, z) = \frac{1}{4\pi}\int_{z+\Delta z}^{\infty} {\rm d}z'\,\frac{{\rm d}l}{{\rm d}z'}\,\left(\frac{1+z}{1+z'}\right)^3\,j\left(E\,\frac{1+z'}{1+z}, z'\right)\,{\rm e}^{-\tau}, \tag{5}$$

where the cosmological proper line element at redshift z' is

$$\frac{{\rm d}l}{{\rm d}z'} = \frac{c}{H_0}\,\frac{1}{1+z'}\,\frac{1}{[\Omega_{\rm M}(1+z')^3 + \Omega_\Lambda]^{1/2}}, \tag{6}$$

and $\tau = \tau(E, z, z')$ is the optical depth effectively crossed by a photon emitted at redshift z' and reaching redshift z with an energy E,

$$\tau \equiv \tau(E, z, z') = \int_z^{z'} {\rm d}\tilde{z}\,\frac{{\rm d}l}{{\rm d}\tilde{z}}\,\sigma\left(E\,\frac{1+\tilde{z}}{1+z}\right)\,n_{\rm B}(\tilde{z}). \tag{7}$$

The definition of a cosmological background would require that in equation (5) $\Delta z = 0$; but this is not appropriate for our purposes. In

[2] If primordial BHs form in clusters (typically) of $N_{\rm cl}$ BHs, the probability that at least one of them is in an active state is $1 - (1-y)^{N_{\rm cl}}$ (rather than y); so $\mathcal{C} \simeq N_{\rm cl}\,y/[1 - (1-y)^{N_{\rm cl}}]$. In the following, we will use $\mathcal{C} = 10$ for models where BH clustering should be strong; this corresponds to $N_{\rm cl} \simeq 330(160)$ for $y = 0.03(0.06)$.

[3] $\mathcal{L}$ is chosen to be the emissivity (per cm^3) when the BH density is equal to 1 M$_\odot$ per comoving Mpc^3 and BHs are assumed to accrete with efficiency 0.1. Thus, it is equal to $0.1 \times 1.3 \times 10^{38}$ (erg s^{-1} M$_\odot^{-1}$) $\times$ [3.086×10^{24} (cm Mpc^{-1})]$^{-3}$.

fact, as we already mentioned, we will be looking at regions outside the ionized 'bubbles' produced by the first luminous sources. Thus, we will examine the effects of the radiation background on baryons quite removed from any particular source (we will refer to such baryons as the 'neutral-IGM' baryons), that is, at a distance of the order of $d/2$. This is irrelevant for photons with long mean free paths [$\lambda(E, z) \gtrsim d/2$], but is of fundamental importance for photons with $\lambda \ll d/2$, which are absorbed in the vicinity of the BHs. In short, we start the redshift integration in equation (5) from $z + \Delta z$ (where Δz is chosen so as to skip the integration over distances $\leqslant d/2$), rather than from z.

From the background spectrum $\phi(E, z)$ we can easily obtain the energy input per baryon due to the absorption of background photons at redshift z,

$$\epsilon(z) = 4\pi \int \mathrm{d}E\, J(E, z)\, \sigma(E). \tag{8}$$

It must be noted that our use of the cross-section (2) in the estimates of τ (equation 7) and of ϵ (equation 8) might induce two opposite errors. First of all, τ is overestimated (and J underestimated) when a significant fraction of the cosmic volume is ionized. On the other hand, when the absorbing medium is not completely neutral, we overestimate the fraction of radiative energy which is actually intercepted by the baryons. The former effect leads to a moderate underestimation of ϵ, starting at relatively high redshifts; the latter might lead to a large overestimation of ϵ, but only for models where the IGM ionized fraction becomes quite large. We neglect both effects in our calculations: our results will generally be mild underestimates of the BH effects, except in the cases where the ionized fraction becomes large (a condition where we will significantly overestimate the BH effects).

The energy input must be split into a fraction $f_{\rm ion}$ going into ionizations, a fraction $f_{\rm heat}$ going into heating, and a fraction $f_{\rm exc}$ going into excitations. These fractions actually depend on the energy E of the absorbed photon; but Shull & van Steenberg (1985) determined that, for all $E \gtrsim 100\,\mathrm{eV}$, they are reasonably fitted by the expressions[4]

$$f_{\rm heat} = 0.9971\left[1 - \left(1 - x_{\rm H}^{0.2663}\right)^{1.3163}\right], \tag{9}$$

$$f_{\rm ion} = 0.3908\left(1 - x_{\rm H}^{0.4092}\right)^{1.7592}, \tag{10}$$

$$f_{\rm exc} = 0.4766\left(1 - x_{\rm H}^{0.2735}\right)^{1.5221}, \tag{11}$$

where $x_{\rm H}$ is the hydrogen ionization fraction ($x_{\rm H} = n(\mathrm{H}^+)/[n(\mathrm{H}^0) + n(\mathrm{H}^+)]$). As can be seen in Figs 1 and 2, the contribution of photons with $E < 100\,\mathrm{eV}$ to the background is small or negligible (in the absence of reionization, the mean free path of 100-eV photons exceeds $\sim$1 comoving Mpc and becomes comparable with d only at $z \lesssim 5$): so the use of these energy-independent functions is legitimate.

2.2 Model parameters

In the above section, we have seen how we can obtain an estimate of the cosmological X-ray background produced by primordial BHs, and of the energy it can inject in the IGM. Such estimate mainly depends on three input quantities: the evolution of the cosmological density of BHs $\rho_{\rm BH}(z)$, the duty cycle y, and the typical spectral

[4] We report the expressions which are given for H, and neglect the small correction due to the presence of He.

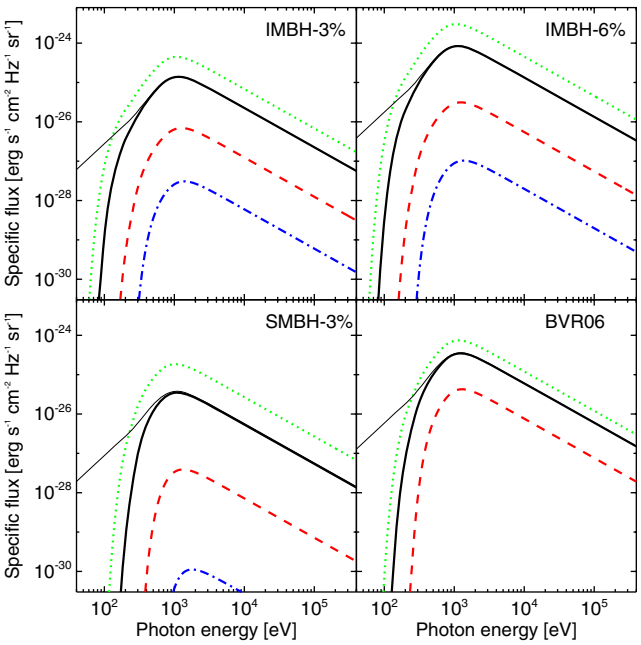

Figure 1. Spectrum of the background produced by primordial accreting BHs and seen by a neutral-IGM baryon in the four BH growth history scenarios (IMBH-3 per cent: top left-hand panel; IMBH-6 per cent: top right-hand panel; SMBH-3 per cent: bottom left-hand panel; BVR06: bottom right-hand panel) at various redshifts ($z = 8$: thick dotted line; $z = 10$: thick solid line; $z = 15$: thick dashed line; $z = 20$: thick dot–dashed line), assuming a PL1 spectrum for the BH emission. The thin solid line shows the spectrum we would obtain at $z = 10$, had we assumed that $\Delta z = 0$ in equation (5).

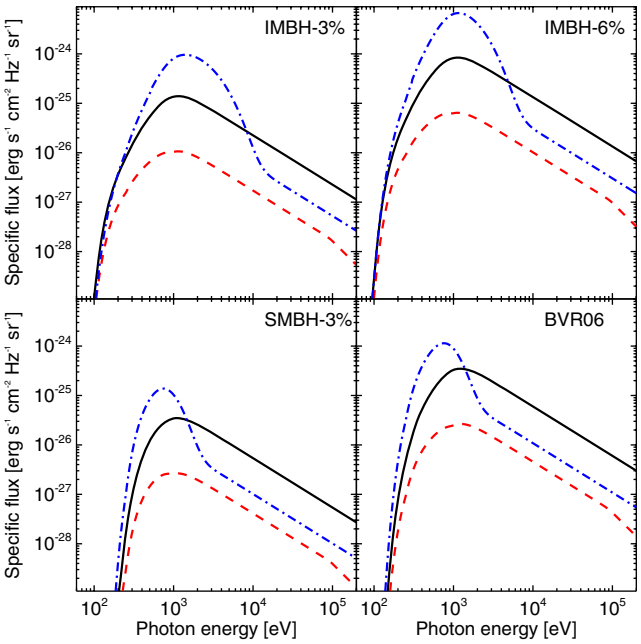

Figure 2. Spectrum of the background produced by primordial accreting BHs, and seen by neutral-IGM baryons at $z = 10$. The four panels refer to the four BH growth history scenarios we consider (IMBH-3 per cent: top left-hand panel;IMBH-6 per cent: top right-hand panel; SMBH-3 per cent: bottom left-hand panel; BVR06: bottom right-hand panel), whereas the different line types refer to three different SEDs for the BH spectra (PL1: solid line; SOS1: dashed line; MC01: dot–dashed line).

Table 1. Parameters of the BH growth model histories.

Model	$\rho_{\rm BH}{}^a$	$\langle M_{\rm BH}\rangle{}^b$	y^c	$\mathcal{C}$	$z_{\rm s}$
IMBH-3 per cent	$10^{6.75-0.275z}$	$10^{3.5-0.05z}$	0.03	10	30
IMBH-6 per cent	$10^{7.5-0.3z}$	$10^{5-0.1z}$	0.06	10	30
SMBH-3 per cent	$10^{7.25-0.375z}$	$10^{6.5-0.05z}$	0.03	1	30
BVR06[d]	$10^{5.675-0.1875z}$	10^{6}	0.10	1	18

[a]In solar masses per cubic comoving Mpc. [b]In solar masses. [c]Consistent with the assumptions of the underlying models. [d]Fig. 2 of BVR06 does not show the $\rho_{\rm BH}$ evolution for $z < 10$; for this reason, at such redshift we will extrapolate the above formula.

shape of an active BH, $F(E)$. The evolution of the BH average mass $\langle M_{\rm BH}\rangle(z)$, and the clustering factor $\mathcal{C}$ have much smaller effects.

2.2.1 BH growth history

There exist several models (e.g. RO04; BVR06; Z07+) predicting the evolution of the BH mass density in the early Universe. Here we will discuss three different histories which are reasonable approximations of the models IMBH-3 per cent, IMBH-6 per cent, and SMBH-3 per cent discussed in Z07+ (see their fig. 8), and of one of the models in BVR06 (duty cycle 0.1, Mestel disc; from their fig. 2). The two IMBH models (IMBH-3 per cent and IMBH-6 per cent) assume that primordial BHs with mass $\sim 100\,{\rm M}_\odot$ form in small (10^6– $10^7\,{\rm M}_\odot$) and numerous haloes, where H_2 cooling is efficient; the SMBH-3 per cent and the BVR06 models, instead, assume that primordial BHs of large mass ($\gtrsim 10^5\,{\rm M}_\odot$) form in larger ($10^8$– $10^9\,{\rm M}_\odot$) and rarer haloes cooled by atomic H. In all the four cases, we will adopt the simple power-law approximations of the Z07+ and BVR06 results which are given in Table 1. Such power laws provide good fits to all the original models for $z \geqslant 10$, whereas at lower redshifts they are either a reasonable extrapolation (for BVR06), or give a slight-to-moderate underestimate of the predictions of the Z07+ models. Table 1 lists also the other parameters defining the BH growth histories: the duty cycle y is by far the most important, whereas our results are relatively insensitive to the assumptions on $\langle M_{\rm BH}\rangle(z)$ and $\mathcal{C}$. This is quite fortunate as the value of y is intrinsic in our reference models, whereas none of them provides a simple estimate of the other parameters. The values given in Table 1 are guesses based on the general properties of the reference models, and on the notion that the typical BH mass should increase with time (especially when $\rho_{\rm BH}$ grows fast).

Furthermore, we assume that before a certain redshift $z_{\rm s}$ ($z_{\rm s} = 30$ for the evolutions taken from Z07+, $z_{\rm s} = 18$ for the one from BVR06) the BH density (and emissivity) is 0.

2.2.2 BH spectral energy distribution

We experiment with three different types of BH spectral energy distributions (SEDs): simple power laws $F(E, z) = F_\alpha(E)$, a template $F(E, z) = F_{{\rm SOS},\alpha}(E)$ introduced by Sazonov, Ostriker & Sunyaev (2004), and a multicomponent spectrum which is the sum of a multicolour blackbody and a power-law spectrum (see Shakura & Sunyaev 1973; Salvaterra et al. 2005), $F(E, z) = F_{{\rm MC},\Phi}(E, z)$.

Power laws are characterized by their slope α, and are assumed to be

$$F_\alpha(E) = \begin{cases} E^{-\alpha} & 0.01 < E < 10^6\,{\rm eV} \\ 0 & \text{otherwise.} \end{cases} \quad (12)$$

In the following, we will consider the power law with $\alpha = 1$ (hereafter PL1 SED) as our reference spectrum.

The spectral template by Sazonov et al. (2004) is characterized by the slope in the 1–100 keV range, and its exact shape is

$$F_{{\rm SOS},\alpha}(E) = \begin{cases} C_0 & 0.1 < E \leqslant 10\,{\rm eV} \\ E^{-1.7} & 10 < E \leqslant 10^3\,{\rm eV} \\ C_1 E^{-\alpha} & 10^3 < E \leqslant 10^5\,{\rm eV} \\ C_2 E^{-1.6} & 10^5 < E < 10^6\,{\rm eV} \\ 0 & \text{otherwise,} \end{cases} \quad (13)$$

where the constants $C_1 = 10^{3(\alpha-1.7)}$ and $C_2 = 10^{2.9-2\alpha}$ are chosen so as to ensure continuity, and the constant $C_0 \simeq 0.1607$ ensures that the fraction of the BH luminosity which goes into photons with $E \leqslant 10\,{\rm eV}$ is the same as in the complete Sazonov et al. (2004) template (i.e. about 0.85), even though we are not interested in the details of their model for $E \leqslant 10\,{\rm eV}$. In this paper, we considered the case $\alpha = 1$ (SOS1 SED): we chose such a relatively steep value (Sazonov et al. 2004 suggest values of about 0.7–0.8) because such SED is intended to show what happens with the steepest spectrum reasonably expected from BHs. However, our results depend only weakly on this index.

Finally, in the multicomponent SED, the multicolour blackbody component is $\propto E^{1/3}$ and dominates up to a peak energy

$$E_{\rm p} \simeq 3000\,{\rm eV}\left(\frac{M_{\rm BH}}{{\rm M}_\odot}\right)^{-1/4}. \quad (14)$$

Above that the multicolour blackbody is exponentially cut-off, and the power-law component ($\propto E^{-1}$) emerges, as described in Shakura & Sunyaev 1973 (see also Salvaterra et al. 2005 for an application to a context similar to the one we are considering):

$$F_{{\rm MC},\Phi}(E, z) = \begin{cases} E^{\frac{1}{3}} {\rm e}^{-\frac{E}{3E_{\rm p}}} & 0.01 < E \leqslant E_{\rm p} \\ E^{\frac{1}{3}} {\rm e}^{-\frac{E}{3E_{\rm p}}} + A_\Phi E^{-1} & E_{\rm p} < E \leqslant 10^6\,{\rm eV} \\ 0 & \text{otherwise.} \end{cases} \quad (15)$$

A_Φ is chosen so that the energy in the power-law spectral component is equal to a fraction Φ of the energy in the multicolour blackbody spectral component. Φ is usually taken to be $\lesssim 1$, and we will consider the case $\Phi = 0.1$ (MC01 SED), which is practically indistinguishable from all the cases with lower Φ, and quite similar to the case with $\Phi = 1$, too. As we substitute $M_{\rm BH}$ with $\langle M_{\rm BH}\rangle(z)$ inside equation (14), we note that this spectral shape is slightly dependent on redshift.[5]

For all the considered spectral shapes, we chose to assume that the BH emissivity at energies below 0.01 eV or above 10^6 eV is 0. Such choice prevents numerical problems, and does not significantly affect our results.

2.3 Results

In Fig. 1, we show the redshift evolution of the spectrum of the background radiation produced by primordial BHs and reaching a

[5] The low-energy tail of a modified blackbody spectrum is expected to be $\propto E^2$. We neglect such slope change, as only a small fraction of the BH luminosity is emitted in this region of the spectrum. We also note that the exponential constant was chosen to be $3E_{\rm p}$ in order to ensure that the multicolour blackbody component actually has a (broad) peak at $E = E_{\rm p}$, as described in Salvaterra et al. (2005).

neutral-IGM baryon. In that figure, we consider all the different BH growth histories, but only the PL1 SED. The background level grows with time, as could be expected when we remember that the BH density, the average distance among BHs, and the IGM density all evolve in a background-enhancing direction. In all the considered growth scenarios, the spectra peak at $E \sim 1$ keV at all redshifts: above this peak the spectrum is almost unabsorbed (i.e. the specific flux decreases in the same way as the input spectrum), whereas the spectrum at energies below the peak is shaped by the cut-off due to the IGM absorption. Such absorption cut-off slowly moves to lower energies. It is also interesting to look at the thin solid line, which illustrates the effect of using $\Delta z = 0$ in equation (5): as expected, the high energy part of the spectrum does not change, while the sharp cut-off at low energies is replaced by a much milder power-law decline.

When comparing different BH growth histories in Fig. 1, it is clear that the normalization of the background spectrum is related to the value of the product $(y \times \rho_{\rm BH})$ at the relevant z. Instead, the sharpness of the low-energy cut-off depends on the geometrical properties of the BH spatial distribution: in models with large values of $\langle M_{\rm BH}\rangle$ the cut-off is very sharp, whereas it is a bit more gentle for IMBH models with low $\langle M_{\rm BH}\rangle$. This is important because the low energy part of the spectrum, albeit accounting only for a small fraction of the total energy in the background, is absorbed with quite high efficiency and is a major contributor to the energy input ϵ.

In Fig. 2, we show the spectrum of the background radiation at a fixed redshift, $z = 10$, while varying the BH SED. It is clear that 'flat' (PL1, MC01) SEDs produce larger backgrounds than 'steep' (SOS1) SEDs, simply because a larger fraction of their luminosity is emitted in the energy range ($E \gtrsim 100$–1000 eV) where incomplete (or negligible) absorption allows the build-up of the background. This is particularly clear for the multicomponent SEDs, that produce a quite prominent bump in a broad energy range around the 1 keV peak of the spectrum. Even if the peak of the background specific flux is never far from ∼1 keV, it is possible to discern some trends: the SOS1 SED tends to peak at slightly lower energies than the PL1 SED, whereas the position of peak of the MC01 SED depends on the chosen BH growth scenario, simply because its peak energy $E_{\rm p}$ depends on the typical BH mass.

Finally, in Fig. 3 we show the total energy input per baryon as a function of redshift. Such a quantity is well correlated with the intensity of the background spectrum, especially at low energies. Thus, it increases with time, and the SED with the highest low-energy component (MC01) gives the maximum energy input. We also compare the energy input from the reference PL1 SED with that from an otherwise identical model where we assumed that $\Delta z = 0$ in equation (5). This is useful to check the effects of our assumption about Δz, and also gives us a rough estimate of the level of the spatial fluctuations of the energy input. The difference usually amounts to a factor of $2 - 3$, even if it might be larger for the SMBH-3 per cent and the BVR06 growth histories, especially at high z.

We note that the model where the energy input from BHs is maximum is the one where the IMBH-6 per cent accretion history is combined with the MC01 SED. In the following, we will refer to such combination as the 'extreme' model, since it leads to the strongest BH feedback effects (and is also close to the constraints from the unresolved X-ray background; see below). On the other hand, we will also consider the IMBH-3 per cent + PL1 model (i.e. the one combining an IMBH-3 per cent history with a PL1 SED) as a 'fiducial' case.

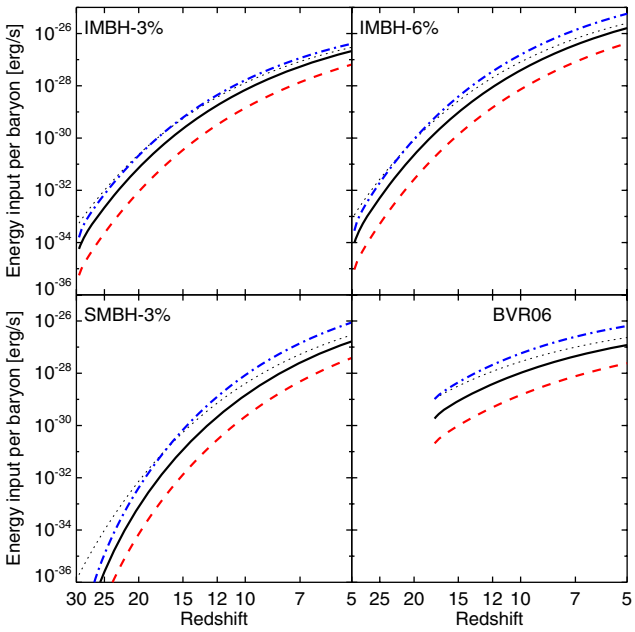

Figure 3. Redshift evolution of the total energy input per neutral-IGM baryon due to the background produced by primordial BHs. As explained in the caption of Fig. 2, the four panels refer to the four considered BH growth histories, and each line type refers to a different assumed BH spectrum. We also show the energy input from BHs with a PL1 SED, had we assumed that $\Delta z = 0$ in equation (5) (thin dotted line).

2.3.1 *Constraints from the unresolved X-ray background*

As a consistency check, we looked at whether our models are compatible with measurements of the unresolved X-ray background from Bauer et al. (2004; hereafter B04), and from Hickox & Markevitch (2007; hereafter HM07).

For such comparison, we obtained the spectrum of the background produced by the BH emission at a redshift $z_{\rm drop}$, we integrated it in the relevant energy band, and we redshifted it to $z = 0$ assuming no absorption.

Such a calculation implies that, at $z \leqslant z_{\rm drop}$, the emissivity due to BHs is 0. This is a quite crude assumption, but it must be remarked that observations (Steidel et al. 2002) suggest that the duty cycle declines with redshift (reaching $y \sim 10^{-3}$ at $z = 0$), and that several theoretical models include a variation of y (e.g. in model M3 of RO04 $y = 1$ at $z \gtrsim 14$, but $y = 10^{-3}$ at $z \lesssim 7$). It is also possible that at redshifts $\lesssim$5–7 an increasing fraction of the BH sources are detected as resolved AGN sources. We also stress that a fraction of IMBHs are expected to merge into larger SMBHs or to be ejected from the parent haloes as a consequence of three-body encounters (see e.g. Volonteri et al. 2002, 2003). In these cases, the IMBHs no longer contribute to the X-ray background. As our model does not account for these effects, it represents a strong upper limit for the X-ray background from IMBHs.

The results of the comparison are listed in Table 2, where we generally adopted $z_{\rm drop} = 5$. It can be seen that two of our models (IMBH-6 per cent growth history, combined with either a PL1 or a MC01 SED) exceed the observed background in at least one band. For such cases (and also for the IMBH-3 per cent + MC01 case, where the contribution from BHs exceeds half of the unresolved X-ray background in the 0.5–2 keV band), we also list the result we would obtain with $z_{\rm drop} = 6$ or 7, which clearly show that the

Table 2. Fraction of the unresolved X-ray background which in our models is due to BH emission at $z \geqslant z_{\rm drop}$, in various bands. The numbers in parenthesis are lower limits, obtained from the assumption that the actual X-ray background is 1σ higher than the central values. The cases where the emission from our models exceeds the unresolved background are in bold face.

Model	$z_{\rm drop}$	0.5–2 keV[a]	2–8 keV[b]	1–2 keV[c]	2–5 keV[d]	0.65–1 keV[e]
IMBH-3 per cent + PL1	5	0.32(0.21)	0.19(0.10)	0.37(0.26)	0.42(0.13)	0.078(0.065)
IMBH-3 per cent + SOS1	5	0.024(0.016)	0.014(0.008)	0.028(0.020)	0.031(0.010)	0.006(0.005)
IMBH-3 per cent + MC01	5	0.67(0.44)	0.043(0.023)	0.24(0.17)	0.096(0.030)	0.21(0.18)
IMBH-3 per cent + MC01	6	0.18(0.11)	0.014(0.008)	0.057(0.041)	0.031(0.010)	0.054(0.045)
IMBH-3 per cent + MC01	7	0.046(0.033)	0.005(0.003)	0.016(0.011)	0.011(0.003)	0.015(0.012)
IMBH-6 per cent + PL1	5	**2.5(1.7)**	**1.5(0.82)**	**2.9(2.1)**	**3.3(1.0)**	0.63(0.52)
IMBH-6 per cent + PL1	6	0.79(0.51)	0.47(0.25)	0.92(0.65)	**1.0(0.32)**	0.19(0.16)
IMBH-6 per cent + PL1	7	0.26(0.17)	0.16(0.084)	0.30(0.21)	0.34(0.10)	0.064(0.053)
IMBH-6 per cent + SOS1	5	0.19(0.13)	0.12(0.062)	0.22(0.16)	0.25(0.078)	0.048(0.040)
IMBH-6 per cent + MC01	5	**1.1(0.71)**	0.33(0.18)	0.65(0.46)	0.72(0.22)	0.24(0.20)
IMBH-6 per cent + MC01	6	0.29(0.19)	0.10(0.055)	0.20(0.14)	0.23(0.069)	0.063(0.052)
IMBH-6 per cent + MC01	7	0.085(0.055)	0.034(0.018)	0.067(0.062)	0.075(0.023)	0.018(0.015)
SMBH-3 per cent + PL1	5	0.26(0.17)	0.16(0.085)	0.30(0.22)	0.34(0.11)	0.065(0.054)
SMBH-3 per cent + SOS1	5	0.020(0.13)	0.012(0.006)	0.023(0.016)	0.026(0.008)	0.005(0.004)
SMBH-3 per cent + MC01	5	0.048(0.031)	0.029(0.016)	0.055(0.039)	0.063(0.019)	0.012(0.010)
BVR06 + PL1	5	0.30(0.19)	0.18(0.097)	0.35(0.25)	0.39(0.12)	0.074(0.061)
BVR06 + SOS1	5	0.023(0.015)	0.014(0.007)	0.027(0.019)	0.030(0.009)	0.005(0.004)
BVR06 + MC01	5	0.054(0.035)	0.032(0.018)	0.063(0.044)	0.071(0.022)	0.013(0.011)

[a]Flux in the 0.5–2 keV band, normalized to a background level of $2.59(4.00) \times 10^{-9}$ erg s^{-1} cm^{-2} sr^{-1} (from the combination of the B04 unresolved fraction, and the Moretti et al. 2003 total X-ray background).
[b]Flux in the 2–8 keV band, normalized to a background level of $4.35(8.05) \times 10^{-9}$ erg s^{-1} cm^{-2} sr^{-1}, (from the combination of the B04 unresolved fraction, and the De Luca & Molendi 2004 total X-ray background).
[c]Flux in the 1–2 keV band, normalized to a background level of $1.12(1.58) \times 10^{-9}$ erg s^{-1} cm^{-2} sr^{-1} (from HM07).
[d]Flux in the 2–5 keV band, normalized to a background level of $1.31(4.26) \times 10^{-9}$ erg s^{-1} cm^{-2} sr^{-1} (from HM07).
[e]Flux in the 0.65–1 keV band, normalized to a background level of $3.28(3.94) \times 10^{-9}$ erg s^{-1} cm^{-2} sr^{-1} (from HM07).

constraints from the X-ray background can be easily satisfied also by these models, provided that $z_{\rm drop} \gtrsim 6$. Thus, we note that the choice of $z_{\rm drop}$ (and, in general, the fate of IMBHs in the lower redshift range we consider) is quite crucial for our models. In the rest of this paper, we will use $z_{\rm drop} = 5$ for all the models, and our plots will extend to such redshift.

3 INFLUENCE ON THE IGM EVOLUTION

We looked at the effects of the energy input due to the background radiation produced by primordial BHs on the thermal and chemical evolution of the IGM. We employed a simplified version of the code described in Ripamonti, Mapelli & Ferrara (2007; hereafter RMF07; but see Ripamonti et al. 2002, and Ripamonti 2007 - hereafter R07 - for more detailed description of this code), in order to look at the evolution of the IGM under the influence of the energy input we calculated in the previous section.

Such a code follows the gas thermal and chemical evolution. The chemistry part deals with 12 chemical species (H,^{0} H,$^+$ H,$^-$ D,^{0} D,$^+$ He,^{0} He,$^+$ He,$^{++}$ H$_2$ H$_2^+$ HD and e$^-$), and includes all of the reactions involving these species which are listed in the Galli & Palla (1998) minimal model for the primordial gas, plus some important extension (e.g. it considers the ionizations and the dissociations due to the energy input we are introducing). The thermal part includes the cooling (or heating, if the matter temperature is lower than the CMB temperature) due to molecules (H$_2$ and HD), to the emission from H and He atoms, to the scattering of CMB photons off free electrons, and to bremsstrahlung radiation. Furthermore, it accounts for the cooling/heating due to chemical reactions, and for the heating due to the energy input we are considering.[6]

3.1 IGM ionization and temperature

Figs 4 and 5 show the effects of the BH emission upon the ionization level (in particular, the hydrogen ionized fraction $x_{\rm H} = n({\rm H}^+)/[n({\rm H}^0) + n({\rm H}^+)]$) and the temperature of the IGM $T_{\rm k}$ (all these quantities are calculated outside the ionized bubbles close to radiation sources). In all the models, we consider, the BH emission starts altering the neutral IGM at $z \sim 15$–20. After that there is a steady increase in both $x_{\rm H}$ and $T_{\rm k}$. The increase of $x_{\rm H}$ stops only when the IGM is completely ionized (however, such condition is reached only in the most extreme of our models, and only at a redshift $\sim$6). Instead, $T_{\rm k}$ stops increasing once it reaches a level ($\sim 10^4$ K), where atomic cooling is important: in the models where BH emission is assumed to be strongest (IMBH-6 per cent with MC01 spectrum) this happens at $z \sim 10$, but $z \sim 6$–8 is a more typical range.

It must be noted that in the lower redshift range we consider (say $z \lesssim 10$) our models start suffering from several problems. First of all, the energy input we employ is calculated for a neutral medium, whereas in some of our models $x_{\rm H} \gtrsim 0.5$ already at $z \sim 7$–8. We are

[6] Other than introducing the energy input as calculated in the previous section, the code differs from the version described in RMF07 because we introduced the cooling through He lines and bremsstrahlung (the rates were taken from Anninos et al. 1997), and we splitted the energy input into the heating, ionization and excitation components by using the expressions given in equation (11), rather than the Chen & Kamionkowski (2004) approximations.

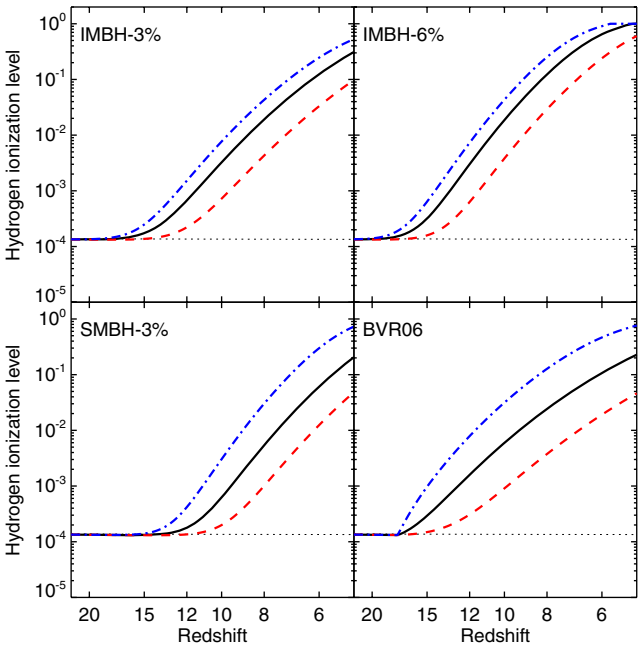

Figure 4. Redshift evolution of the hydrogen ionization fraction $x_{\rm H}$. The order of the panels and the meaning of the various line types are the same as in Fig. 2, except for the thin dotted line, which represents the ionization evolution in a model without any BH emission.

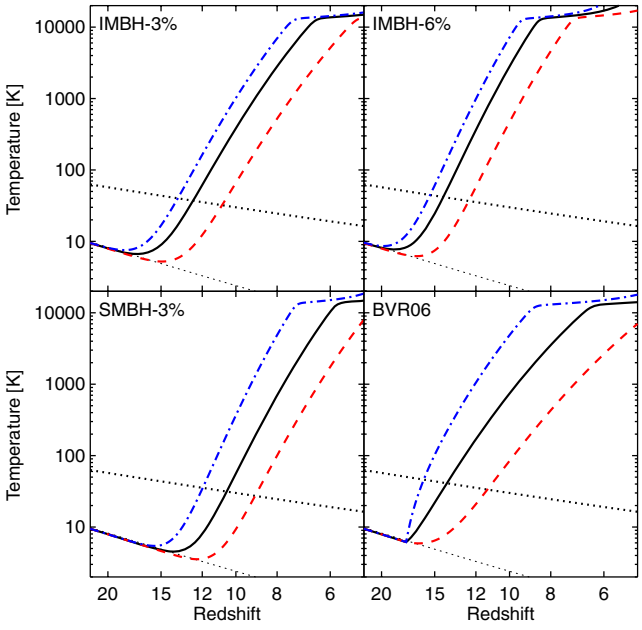

Figure 5. Redshift evolution of the IGM temperature $T_{\rm k}$ in regions outside ionized bubbles. The order of the panels and the meaning of the various line types are the same as in Fig. 2, except for the thin dotted line, which represents the temperature evolution in a model without any BH emission, and for the thick dotted line representing the CMB temperature.

then overestimating the energy input.[7] Secondly, we are assuming that the IGM density remains constant at its average unperturbed cosmological value, whereas this approximation becomes increasingly problematic as structures start to form. Third, there might be some level of metal enrichment (altering both the heating and the cooling rates) even in regions which are far away from the most luminous sources. Finally, we are completely neglecting the contribution to heating and reionization which is due to stars, which is likely to be substantial at relatively low redshifts. However, our calculations should still be reasonably accurate until the end of the so-called 'overlap' phase of reionization (probably not far from $z \sim 7$–8, see Section 5.1), provided that they are taken to represent conditions in regions which were not yet ionized.

3.2 CMB angular spectrum

The cosmic heating and the contribution to reionization due to BHs might also leave some imprint on the CMB spectra. In order to study this effect, we implement ionization and gas temperature evolution due to BHs in the version 4.5.1 of the public code CMBFAST (Seljak & Zaldarriaga 1996; Seljak et al. 2003).

Fig. 6 shows the temperature–temperature (TT), polarization–polarization (EE) and temperature–polarization (TE) spectra of the CMB in the case in which the contribution from BHs is accounted for. In particular, the 'extreme' case (IMBH-6 per cent + MC01, solid line) and the 'fiducial' one (IMBH-3 per cent + PL1, dashed line) are shown. They are also compared with the spectra obtained without contributions from stars and/or BHs (thin dot–dashed line) and with the spectra derived assuming Thomson optical depth $\tau_{\rm e} = 0.09$ and a sudden reionization at $z \simeq 11$, consistent with the three-year *Wilkinson Microwave Anisotropy Probe* (*WMAP*) data.

As one can expect, no significant differences appear between the four cases in the TT spectrum. The 'fiducial' and the 'extreme' BH model differ from the thin dot–dashed line both in the EE and in the TE spectra, at low multipoles ($l \lesssim 20$). However, the contribution of BHs to the TE and EE spectra, even in the extreme case (IMBH-6 per cent + MC01), is smaller than (or comparable to) the best fit of the three-year *WMAP* data (dotted line). Thus, all the scenarios considered in this paper (even IMBH-6 per cent + MC01) do not violate the limits posed by CMB observations.

Furthermore, the Thomson optical depth which can be directly derived from the ionization history shown in Fig. 4 is $\tau_{\rm e} < 0.07$ ($\tau_{\rm e} = 0.027$ and 0.064 in the 'fiducial' and 'extreme' case, respectively), smaller than the best fit to three-year *WMAP* data ($\tau_{\rm e} = 0.09 \pm 0.03$, Spergel et al. 2007). Thus, our BHs might give a partial contribution to the reionization, but are not its exclusive source, in agreement with previous work (e.g. RO04; Ricotti et al. 2005; Z07+).

[7] The situation is actually quite complicated. The reduction in the heating rate is slower than what could naively be expected [$\epsilon \propto (1 - x_{\rm H})^{-1}$] from the increase of $x_{\rm H}$, because the bulk of the cross-section is due to He, which is harder to strip of its electrons (see e.g. Thomas & Zaroubi 2008). For example, in the 'extreme' model, at redshift 6 $x_{\rm H} \simeq 0.9$, but $x_{\rm He^{++}} \equiv n({\rm He^{++}})/[n({\rm He^0}) + n({\rm He^+}) + n({\rm He^{++}})] \simeq 0.1$, and by using equation (2) we are overestimating the energy input ϵ only by a factor of $\sim$2.5 rather than $(1 - x_{\rm H})^{-1} \sim 10$. Furthermore, the assumption that the IGM is completely neutral also leads to an overestimation of the optical depth τ, and the background radiation (and energy input) is correspondingly underestimated. Our energy input rates are then essentially correct, except for our 'extreme' model at $z \lesssim 7$, where we might be overestimating ϵ by a factor of $\lesssim$2.

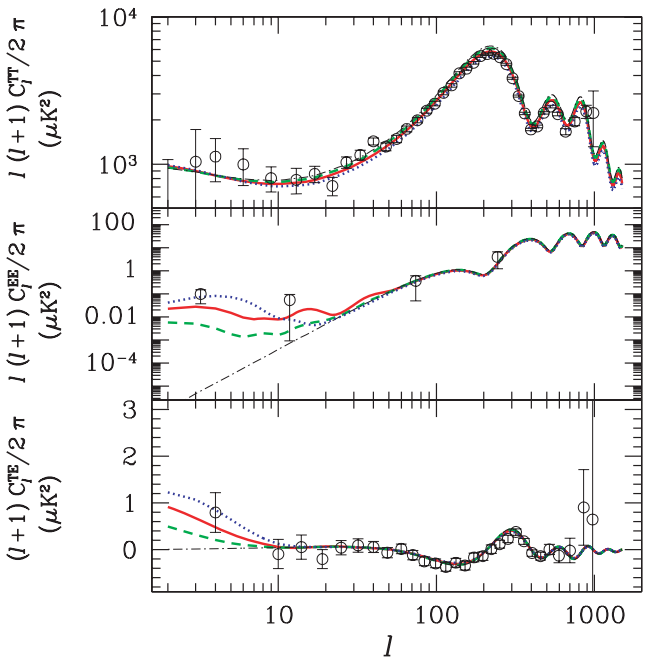

Figure 6. Effects of BH emission upon the CMB angular spectra. TT (top panel), EE (central panel) and TE (bottom panel) spectra are shown. Thick dotted line: CMB spectra derived assuming Thomson optical depth $\tau_e = 0.09$ and a sudden reionization model (consistent with the three-year *WMAP* data); thick solid and dashed lines: CMB spectra derived assuming energy injection from the BHs in the 'extreme' (IMBH-6 per cent + MC01, that is, the case where BH energy input is strongest) and the 'fiducial' (IMBH-3 per cent + PL1) cases, respectively; thin dash–dotted line: CMB spectra derived assuming no reionization and no contribution from BHs.

3.3 21-cm radiation

3.3.1 Basic definitions

The spin temperature of the 21-cm transition can be written as (see e.g. Field 1958, 1959; Kuhlen, Madau & Montgomery 2006; Valdès et al. 2007; Z07+):

$$T_{\rm spin} = \frac{T_* + T_{\rm CMB} + (y_{\rm k} + y_\alpha)T_{\rm k}}{1 + y_{\rm k} + y_\alpha}, \tag{16}$$

where $T_* \equiv 0.068\,{\rm K}$ corresponds to the 21-cm transition energy, $T_{\rm CMB}$ is the CMB temperature, $T_{\rm k}$ is the IGM kinetic temperature, and $y_{\rm k}$ and y_α are the kinetic and Lyman α coupling terms, respectively.

The kinetic coupling term is

$$y_{\rm k} = \frac{T_*}{A_{10}\,T_{\rm k}}\,(C_{\rm H} + C_{\rm e} + C_{\rm p}), \tag{17}$$

where $A_{10} \simeq 2.85 \times 10^{-15}\,{\rm s}^{-1}$ is the Einstein spontaneous emission rate coefficient (Wild 1952), and $C_{\rm H}$, $C_{\rm e}$ and $C_{\rm p}$ are the de-excitation rates due to neutral H, electrons and protons, respectively. They are given by the fitting formulae from Kuhlen et al. (2006) (see also Field 1958, 1959; Smith 1966; Allison & Dalgarno 1969; Nusser 2005; Zygelman 2005):

$$C_{\rm H} \simeq 3.1 \times 10^{-11} \left(\frac{T_{\rm k}}{1\,{\rm K}}\right)^{0.357} {\rm e}^{-\frac{32\,{\rm K}}{T_{\rm k}}}\ {\rm s}^{-1} \tag{18}$$

$$C_{\rm e} \simeq n_{\rm e}\,\gamma_{\rm e} \tag{19}$$

$$C_{\rm p} \simeq 3.2 \left(\frac{n_{\rm p}}{n_{\rm H}}\right) C_{\rm H}, \tag{20}$$

where $n_{\rm H}$, $n_{\rm e}$ and $n_{\rm p}$ are the neutral H, electron and proton number densities, and

$$\log_{10}\frac{\gamma_{\rm e}}{1\,{\rm cm}^3\,{\rm s}^{-1}} \simeq -9.607 + 0.5\log_{10}\frac{T_{\rm k}}{1\,{\rm K}} \times \exp\left[\frac{1}{1800}\left(\log_{10}\frac{T_{\rm k}}{1\,{\rm K}}\right)^{4.5}\right]. \tag{21}$$

The Lyman α coupling term is given by

$$y_\alpha = \frac{16\pi}{27A_{10}}\,\frac{T_*}{T_{\rm k}}\,\frac{\pi {\rm e}^2}{m_{\rm e}\,c}\,f_{12}\,J_0, \tag{22}$$

where e and $m_{\rm e}$ are the electron charge and mass, $f_{12} \simeq 0.416$ is the oscillator strength of the Lyman α transition, and J_0 is the intensity of Lyman α photons which are due to collisional excitations from thermal electrons, to hydrogen recombinations, and to collisional excitations from X-ray energy absorption. J_0 is then

$$J_0 = \frac{hc}{4\pi\,H(z)}\left[n_{\rm e}n_{\rm H}\gamma_{\rm e,H} + n_{\rm e}n_{\rm p}\alpha_{2^2{\rm P}}^{\rm eff} + \frac{n_{\rm B}\epsilon\,f_{\rm exc}}{h\nu_\alpha}\right], \tag{23}$$

where $\gamma_{\rm e,H} \simeq 2.2 \times 10^{-8}{\rm e}^{-(118\,400\,{\rm K})/T_{\rm k}}\ {\rm cm}^3\,{\rm s}^{-1}$ is the collisional excitation rate of neutral H atoms by electron impacts, $\nu_\alpha \sim 2.46 \times 10^{15}$ Hz is the Lyman α frequency, and $\alpha_{2^2{\rm P}}^{\rm eff}$ is the effective recombination coefficient to the 2^2P level (including recombinations to the 2^2P level, plus recombinations to higher levels that end up in the 2^2P level through all possible cascade paths). We adopted a simple fit to the Pengelly (1964) results for $\alpha_{2^2{\rm P}}^{\rm eff}$, assuming case A recombinations:[8]

$$\alpha_{2^2{\rm P}}^{\rm eff}(T_{\rm k}) \simeq 1.67 \times 10^{-13}\,T_4^{-0.91-(2/75)\log_2 T_4}, \tag{24}$$

where $T_4 = T_{\rm k}/(10^4\,{\rm K})$.

Once the spin temperature is known (from equation 16), it is convenient to express the resulting 21-cm radiation intensity as the differential brightness temperature between neutral hydrogen and the CMB, which is an observable quantity:

$$\delta T_{\rm b} \simeq \frac{T_{\rm spin} - T_{\rm CMB}}{(1+z)}\,\tau_{21}(1+\delta_\rho), \tag{25}$$

where $\delta_\rho \equiv (\rho - \bar\rho)/\bar\rho$ is the cosmological density contrast in the considered region (here we will consider only the case $\delta_\rho = 0$), and τ_{21} is the IGM optical depth at an observed wavelength of $21(1+z)$ cm:

$$\tau_{21} \simeq \frac{3c^3hA_{10}}{32\pi\,k_{\rm B}\nu_{21}^2 H(z)}\,\frac{n_{\rm H}}{T_{\rm spin}}, \tag{26}$$

where $k_{\rm B}$ is the Boltzmann constant, and $\nu_{21} \simeq 1.421 \times 10^9$ Hz is the (rest-frame) frequency of the 21-cm line.

3.3.2 Results for pure BH coupling

Fig. 7 shows the redshift evolution of $T_{\rm spin}$, under the assumption that only the radiation produced by BHs is important.

In all these models, $T_{\rm spin}$ remains very close to $T_{\rm CMB}$ (and to the predictions of models with no BH emission) until $z \sim 9$–15, that is, until $T_{\rm k}$ finally becomes much larger than $T_{\rm CMB}$. After that, the difference between $T_{\rm spin}$ and $T_{\rm CMB}$ becomes significant, and in models with strong BH emission it can amount to ∼90 K. Apart

[8] Results for case B recombinations differ only slightly.

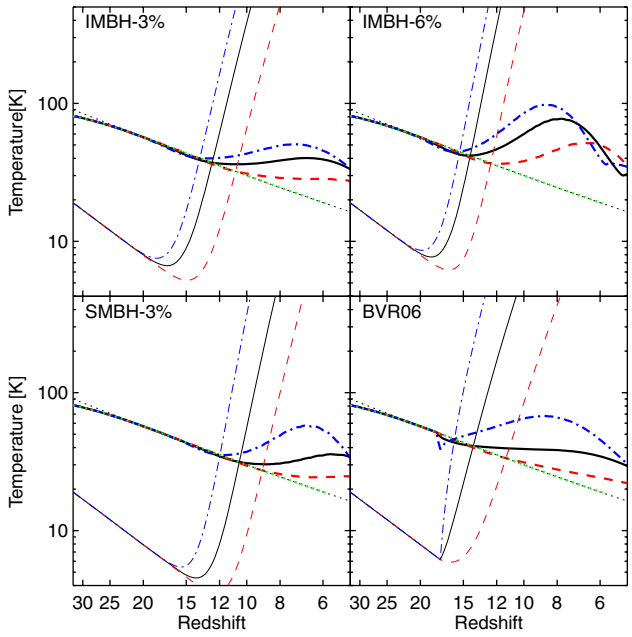

Figure 7. Redshift evolution of the neutral H spin temperature. The order of the panels is the same as in Fig. 2; the dotted line represents the CMB temperature, the thick lines represent the spin temperature, and the thin lines represent the IGM temperature. The continuous lines refer to models with a PL1 SED, the dashed lines to models with a SOS1 SED, and the dot–dashed lines to models with a MC01 SED.

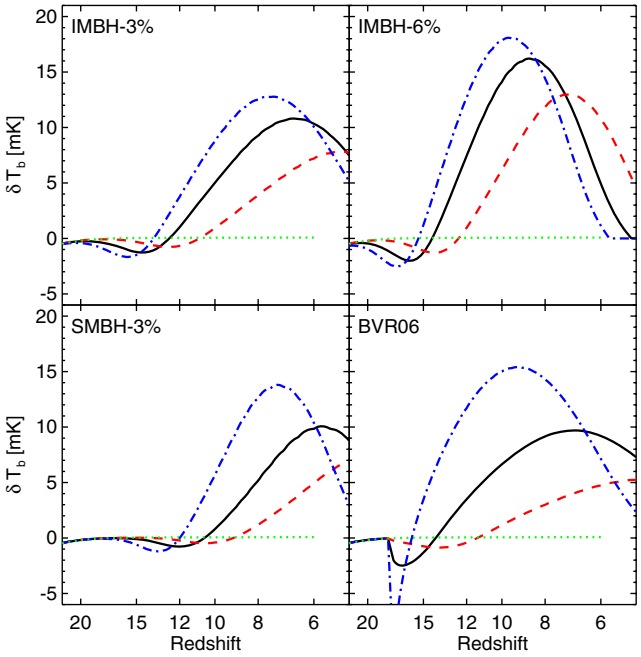

Figure 8. Redshift evolution of the brightness temperature difference with respect to the CMB $\delta T_{\rm b}$. The order of the panels and the meaning of the various line types are the same as in Fig. 2, except for the dotted line, which represents $\delta T_{\rm b}$ for a model without any BH emission.

from the amplitude of this maximum difference, the strength of BH emission also influences the redshift when it is reached: in models with weak BH emission (e.g. most models where a SOS1 SED is assumed), $T_{\rm spin} - T_{\rm CMB}$ keeps increasing, and is largest at the lowest considered redshift (though this maximum is quite low); whereas in models with strong BH emission (e.g. all those where a MC01 SED is assumed) $T_{\rm spin} - T_{\rm CMB}$ reaches a relatively high maximum at $z \sim$ 6–9, slowly decreasing afterwards. The main reason is that in models with high BH emission the ionized fraction easily reaches the regime (at $x_{\rm H} \gtrsim 0.1$), where $f_{\rm exc}$ (and J_0 and y_α with it, as J_0 is dominated by the term due to collisional excitations from X-ray absorption) starts dropping very fast, rather than being approximately constant (see fig. 4 of Shull & van Steenberg 1985).

In Fig. 8, we show the corresponding evolution of the differential brightness temperature $\delta\, T_{\rm b}$. Such evolution essentially mirrors the one of $T_{\rm spin} - T_{\rm CMB}$: it remains close to 0 until $z \sim$ 9–15, and then starts growing, reaching maxima between ∼5 and ∼18 mK, depending on the strength of the BH emission. Again, in models with weak BH emission the maximum is reached at the lowest considered redshift, whereas in the other models it is reached at $z \sim$ 6–9. The main difference with the evolution of $T_{\rm spin} - T_{\rm CMB}$ is that the decline after the maximum is faster, since the high IGM ionization level in models with strong BH emission reduces also τ_{21}.

It must be remarked that such an evolution of $\delta T_{\rm b}$ in the neutral patches of the Universe at $z \lesssim 12$ should be detectable with the new generation of radio experiments, such as LOFAR, MWA, 21CMA and SKA.[9] For example, LOFAR will probe the 21-cm emission emitted from the IGM in the redshift range of 6–11.5 and will be sensitive to scales from a few arcminutes up to few degrees and will be able to statistically detect the 21-cm brightness temperature down to ≈5 mK (de Bruyn, Zaroubi & Koopmans 2007; de Bruyn et al., in preparation). However, we stress that these effects are observable only before the end of the reionization epoch (see Section 5.1).

3.3.3 Results for BH and stellar coupling

In the previous section, we considered the evolution of the 21-cm emission under the effects of BH emission only. But it is largely believed that stellar emission played a fundamental role in the evolution of the primordial Universe: for example, most models of reionization (e.g. RO04, and references therein) assume that the stellar contribution was dominant over the one from BHs. This is supported by observations of the unresolved X-ray background, whose level is difficult to reconcile with the hypothesis that reionization is due to BH emission (e.g. Dijkstra et al. 2004). Furthermore, our models *do* require the presence of stellar radiation, as even the 'extreme' one (IMBH-6 per cent + MC01) is unable to reionize the Universe before $z \sim 6$, and is therefore incompatible with observations of quasars and Lyman α emitters at $z \sim$ 6–7 (Becker et al. 2001; Djorgovski et al. 2001; Fan et al. 2001, 2002, 2003; White et al. 2003; Iye et al. 2006; Kashikawa et al. 2006; Ota et al. 2007).

Since we are looking at the evolution of the IGM in regions which are quite removed from BHs (and, consequently, from the bulk of stellar emission) and are reionized late,[10] the omission of the stellar contribution from our calculations is mostly justified. In fact, the

[9] http://www.lofar.org
http://www.haystack.mit.edu/ast/arrays/mwa/
http://21cma.bao.ac.cn/
http://www.skatelescope.org

[10] It is natural to wonder down to which redshift such neutral regions actually exist. Here, we will simply assume that they survive down to $z \sim 5$, and look into their properties. Such hypothesis will be discussed in Section 5.1.

neutral IGM we are considering is almost perfectly transparent to radiation with frequencies below the H ionization threshold (13.6 eV): such photons can travel cosmological distances, but are unable to significantly affect the IGM. On the other hand, the ionizing photons emitted from stars are typically absorbed at the edge of the ionized regions around stellar sources, since they are not energetic enough to cross significant distances in a neutral IGM: for this reason, their effects are purely local.

Lyman α photons are the only relevant exception. In fact, although the Lyman α cross-section is very high, such photons can scatter many times before exiting the resonance; more importantly, the redshifting of photons with energies slightly higher than 10.2 eV 'into' the resonance ensures a roughly uniform Lyman α radiation field also in neutral regions.

Ciardi & Salvaterra (2007; hereafter CS07) found that the Lyman α radiation field can moderately heat the IGM: the heating rate taken from their models dominates over that of all our models at $z \gtrsim 15$, and takes the IGM temperature to $\gtrsim$30 K at $z \sim 15$–20. On the other hand, at $z \lesssim 10$ the Lyman α heating rate should be much smaller than those of our models.[11] More importantly, CS07 find that for $z \lesssim 27$ the intensity $J_{\alpha,*}$ of the Lyman α background is much higher than the level [$J_{\alpha,\mathrm{coupling}} \sim 10^{-22}\ (1+z)\,\mathrm{erg\,cm^{-2}\,s^{-1}\,Hz^{-1}\,sr^{-1}}$] which should couple T_{spin} to T_{k} rather than to T_{CMB} (see Ciardi & Madau 2003).

In our case, it is reasonable to neglect the heating effects of the Lyman α background, although this will lead us to somewhat underestimate the IGM temperature at $z \gtrsim 15$. But it is very important to add the effects of the Lyman α background to our estimation of T_{spin} (and δT_{b}).

This can be done very easily by modifying equation (16) into

$$T_{\mathrm{spin}} = \frac{T_* + T_{\mathrm{CMB}} + (y_{\mathrm{k}} + y_\alpha + y_{\alpha,*})T_{\mathrm{k}}}{1 + y_{\mathrm{k}} + y_\alpha + y_{\alpha,*}}, \tag{27}$$

where $y_{\alpha,*}$ accounts for the additional coupling due to the Lyman α background due to the stars,[12] and is approximately given by (see CS07):

$$y_{\alpha,*} \sim 10^9 \frac{J_{\alpha,*}\,T_*}{A_{10}\,T_{\mathrm{k}}}. \tag{28}$$

After approximating $J_{\alpha,*}$ with the expression

$$\frac{J_{\alpha,*}(z)}{\mathrm{erg/(cm^2\,s\,Hz\,sr)}} = \begin{cases} 0 & z \geqslant 30 \\ 10^{-18-[0.1(z-10)]} & 30 > z > 10 \\ 10^{-18} & z \leqslant 10, \end{cases} \tag{29}$$

which is a moderate underestimate of the $J_{\alpha,*}$ curves shown in fig. 1 of CS07, we have recalculated the evolution of T_{spin}, and δT_{b}. The results are shown in Figs 9 and 10.

In this case, T_{spin} (Fig. 9) is almost perfectly coupled to the kinetic temperature, and the difference $T_{\mathrm{spin}} - T_{\mathrm{CMB}} \simeq T_{\mathrm{spin}}$ easily reaches the 10^3–10^4 K range. Also δT_{b} (Fig. 10) is affected. Here we focus on the relatively low redshifts which will be explored by 21-cm

[11] The plots in CS07 actually stop at $z = 10$; but it is pretty clear that in their model the IGM temperature is growing at a much slower rate than in our models. It is also worth noting that some of the CS07 assumptions (e.g. the values of the parameters f_{gas} and f_*) are quite extreme, and would result in a very early complete reionization. More realistic assumptions would result in a significant delay in the rise of T_{spin}.

[12] Also BHs produce a Lyman α background; but its intensity is much lower than the one due to stars, and the corresponding coupling term is always much smaller than y_α.

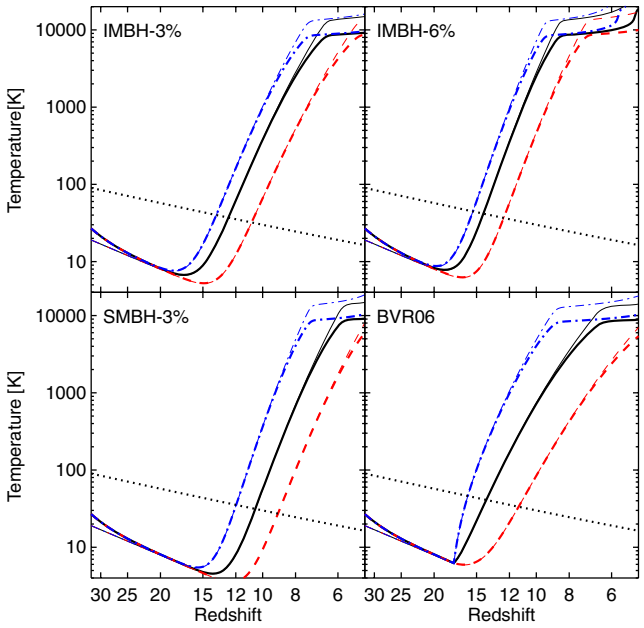

Figure 9. Redshift evolution of the neutral H spin temperature, when the Lyman α coupling due to stellar radiation (but not the stellar radiation heating effects) is kept into account. The order of the panels is the same as in Fig. 2. The dotted line represents the CMB temperature, the thick lines represent the spin temperature, and the thin lines represent the IGM temperature. The continuous lines refer to models with a PL1 SED, dashed lines to models with a SOS1 SED, and the dot–dashed lines to models with a MC01 SED.

experiments (e.g. LOFAR), where the effects of BH emission lead to differential brightness temperatures which can reach 20–30 mK at redshifts $\sim 8-15$. Instead, at high redshifts (say, $z \gtrsim 15$) δT_{b} can reach very high negative values (in the -200 to -300 mK range); but in such redshift range the results of CS07, predicting a minimum value of $\delta T_{\mathrm{b}} \sim -170$ mK at $z \sim 24$ are likely more correct because they include also the the heating effects of the stellar Lyman α background.

We point out that our results, especially those about δT_{b}, depend only weakly from the very high level of $J_{\alpha,*}$ given in the CS07 paper: the effects of lowering $J_{\alpha,*}$ to a more realistic level, e.g. a fraction 0.1 (or even 0.01) of the amount given by equation (29) are a certain reduction (from $\sim$8–10 000 K to 3–5000 K) of the level where T_{spin} reaches a low-redshift 'plateau', and a much smaller change in the evolution of δT_{b}. Our predictions about δT_{b} observations are then quite independent of the assumptions of CS07. Instead, for the model where no BH feedback is included, a reduction by a similar factor in the Lyman α heating rate in the CS07 models would result in a much lower δT_{b} value than shown by the dotted curve in Fig. 10.

4 INFLUENCE ON STRUCTURE FORMATION

In the previous section, we have shown that the energy input from BHs can substantially heat the IGM. In turn, this is likely to affect the formation of galaxies: as the cosmological Jeans mass depends on $T_{\mathrm{k}}^{3/2}$, the baryonic component of small fluctuations might become unable to collapse and form stars because of the temperature increase. But the effects of BH radiation are not limited to the heating, since the increase in the H ionized fraction also enhances the formation of H_2 which is the most important coolant in metal-free gas at temperatures $\lesssim 10^4$ K: such enhancement would facilitate the formation of stars within small haloes. We then investigated

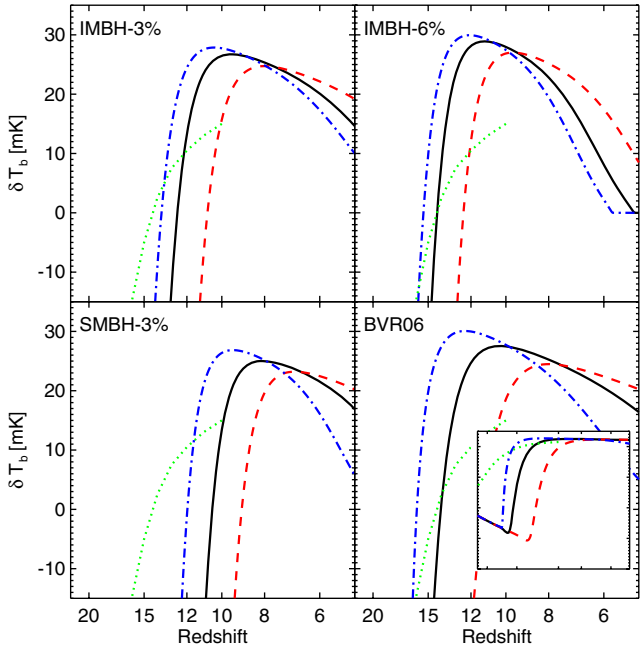

Figure 10. Redshift evolution of the brightness temperature difference with respect to the CMB $\delta T_{\rm b}$, when the Lyman α coupling due to stellar radiation is kept into account. The order of the panels and the meaning of the various line types are the same as in Fig. 2. The inset in the bottom right-hand panel shows the same quantities (for the BVR06 case; the other cases are qualitatively similar) on a much wider $\delta T_{\rm b}$ scale. The dotted line stopping at $z = 10$ comes from fig. 5 (bottom panel, solid line) of CS07, and shows $\delta T_{\rm b}$ for a model with stellar Lyman α coupling and heating, but no BH emission. This line represents an upper limit on $\delta T_{\rm b}$ in the absence of BH heating.

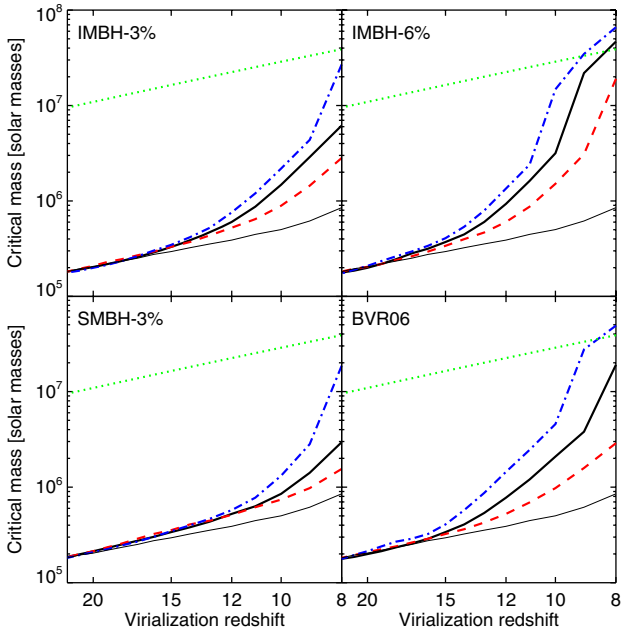

Figure 11. Redshift evolution of the critical mass. The order of the panels and the meaning of the various line types are the same as in Fig. 2, except for the thin continuous line, which represents $M_{\rm crit}$ for a model without any BH emission, and for the dotted line, representing the mass $M_{\rm H}$ of haloes with virial temperature $T_{\rm vir} = 10^4$ K.

the influence of BH energy input on structure formation with a method which accounts for such competing effects, and which was already employed in the RMF07 and R07 papers.

We used the full code (instead of the simplified version used in the previous section) described in Section 3, in order to follow the evolution of spherically symmetric haloes of different masses, virializing at different redshifts. Such evolution took into account all the physics included in the simplified version we already described, plus the treatment of gravity, of the hydrodynamical evolution of the gas, and of the dissociation of H_2 molecules due to Lyman–Werner ($11.2 \leqslant h\nu \leqslant 13.5$ eV) photons emitted by BHs.[13] Dark matter (DM) gravitational effects are included as described in section 2.1.3 of R07: the DM final density profile is assumed to be a truncated isothermal sphere with $\xi = 0.1$ (i.e. the final core radius is assumed to be 1/10 of the virial radius).

4.1 Critical mass

As in the RMF07 and R07, we classified haloes as collapsing if they reach a maximum density larger than $\rho_{\rm coll} = 1.67 \times 10^{-19}\,{\rm g\,cm^{-3}} \simeq 10^5 m_{\rm H}\,{\rm cm^{-3}}$ (a value high enough to suggest that the formation of a luminous object is well under way) in less than an Hubble time after their virialization (at $z_{\rm vir}$), that is, at a redshift $z_{\rm coll} \gtrsim [0.63(1 + z_{\rm vir})] - 1$.

This classification criterion is roughly comparable to the collapse criterion of Tegmark et al. (1997): in analogy with such paper (and with RMF07 and R07), we define the critical mass $M_{\rm crit}(z_{\rm vir})$ as the minimum mass of a collapsing halo virializing at $z_{\rm vir}$.

In Fig. 11, we compare the evolution of $M_{\rm crit}$ which is obtained for each of our BH models with the same evolution in the unperturbed ($\epsilon = 0$ at all redshifts) case, and with the evolution of the mass

$$M_{\rm H}(z_{\rm vir}) \simeq 1.05 \times 10^9\,{\rm M_\odot}\,(1 + z_{\rm vir})^{-3/2} \qquad (30)$$

of haloes with a virial temperature $T_{\rm vir} = 10^4$ K (assuming a mean molecular weight $\mu = 1.23$, as appropriate for a neutral medium), above which the cooling due to atomic H becomes dominant.

The BH energy injection has negligible effects upon $M_{\rm crit}$ for $z_{\rm vir} \gtrsim 15$, but its effects become increasingly important at later times: at $z = 10$ the BH energy input increases $M_{\rm crit}$ by a factor between 1.8 (SMBH-3 per cent + SOS1 model) and 40 (IMBH-6 per cent + MC01 model). At lower redshifts the BH effects are even larger: in the models with the strongest BH feedback, $M_{\rm crit}$ can become $\gtrsim M_{\rm H}$, although the onset of atomic cooling slows down the increase of $M_{\rm crit}$: in such models, BH feedback prevents the formation of stars inside minihaloes cooled by molecules at $z \lesssim 9$.

4.2 Gas retention

RMF07 suggested that one possible feedback effect of the energy input from decaying/annihilating DM particles is to reduce the amount of gas which actually ends up within the potential wells of virialized haloes. As the feedback effects of BHs are much stronger than those of DM decays and annihilations, we looked at whether these same effects are important in our simulations.

To this purpose, we define $f_{\rm ret}$ as the ratio of the mass of gas which is retained inside the virial radius of a halo (at the time when our

[13] For this last effect we use the reaction rate given by Abel et al. 1997 (reaction 27); the flux of photons at 12.87 eV was obtained through the formalism described in Section 2.1, but assuming that photons at frequencies corresponding to the lines of the Lyman series of hydrogen were completely absorbed. No stellar emission was assumed.

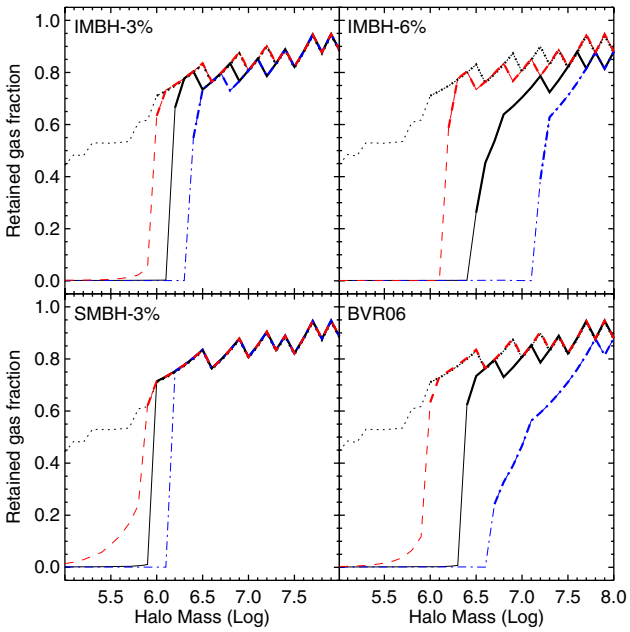

Figure 12. Fraction of gas retained by a halo at the end of our simulations in haloes virializing at $z_{\rm vir} = 10$, as a function of the total halo mass. The order of the panels and the meaning of the continuous, dashed and dot–dashed lines are the same as in Fig. 2; the dotted lines refer to the unperturbed model. The thickness of the line indicates whether a certain halo mass is below (thin line) or above (thick line) the critical mass. The seesaw behaviour for high masses is purely numerical (i.e. due to the discrete number of shells).

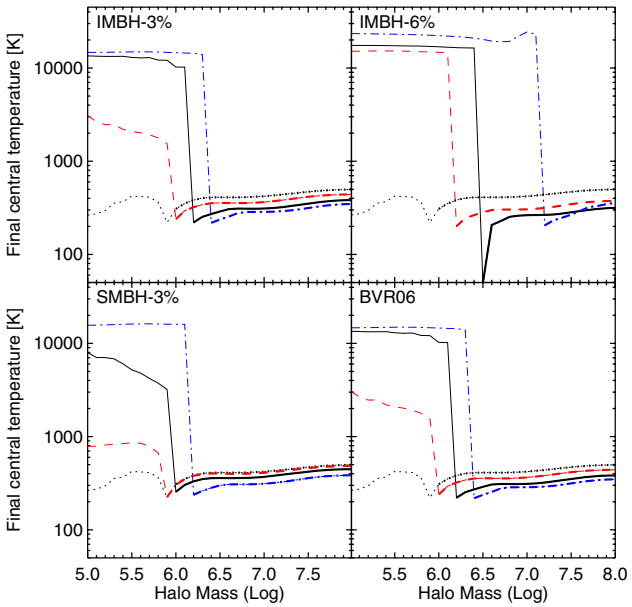

Figure 13. Central gas temperature at the end of our simulations in haloes virializing at $z_{\rm vir} = 10$, as a function of the total halo mass. The order of the panels and the meaning of the continuous, dashed and dot–dashed lines are the same as in Fig. 2; the dotted lines refer to the unperturbed model. The thickness of the line indicates whether a certain halo mass is below (thin line) or above (thick line) the critical mass.

simulations are stopped) with respect to the baryonic mass expected from cosmology. For a halo with total mass $M_{\rm halo}$ and baryonic mass $M_{\rm gas}$:

$$f_{\rm ret} = \frac{M_{\rm gas}}{M_{\rm halo}} \frac{\Omega_{\rm m}}{\Omega_{\rm b}}. \tag{31}$$

In Fig. 12, we show the dependence of $f_{\rm ret}$ upon $M_{\rm halo}$, for haloes virializing at $z_{\rm vir} = 10$ and for all our BH models, plus the unperturbed case.

Generally, models with BH feedback exhibit a sharp transition at $M_{\rm halo} \simeq M_{\rm crit}$, going from $f_{\rm ret} \sim 0$ to $f_{\rm ret} \gtrsim 0.7$, whereas in the unperturbed case $f_{\rm ret}$ increases quite smoothly from ∼0.4 to ∼0.9 (this last value is in good agreement with numerical simulations by Crain et al. 2007). This threshold effect is due to the hydrodynamical effects of the BH heating, combined with the depth of the DM potential well. In fact, the heating induced by the BHs amplifies the pressure gradients and tends to prevent the gas from falling inside the DM potential well. If the DM potential well is below a certain critical value (i.e. if $M_{\rm halo} \lesssim M_{\rm crit}$), the final gas overdensity is generally $\lesssim$10, whereas the DM overdensity is $\gtrsim$1000. On the other hand, if the gravity of a halo is strong enough (i.e. if $M_{\rm halo} \gtrsim M_{\rm crit}$), the heating induced by the BHs cannot counteract the gravitational pull, and the halo will retain most of its gas, which will cool, collapse and form luminous objects.

This is confirmed by Fig. 13, where we show the final temperature of the gas at the centre of haloes virializing at $z_{\rm vir} = 10$, as a function of the halo mass. In haloes with mass $\leqslant M_{\rm crit}$, the gas temperature is much higher, if BH heating is present, than in the unperturbed case, and it is close to the temperature $T_{\rm k}$ of the IGM (1000–10 000 K). For masses $\geqslant M_{\rm crit}$ the final temperature in presence of BH heating is similar to the unperturbed case (200–400 K, much lower than the temperature of the surrounding IGM), as the gas in the centre of the halo was able to condense and cool. The transition in the case of the gas temperature is even sharper than in the case of $f_{\rm ret}$, probably because the density dependence of the cooling rate[14] will lead to a 'runaway' cooling as soon as the density starts to increase.

Fig. 12 also shows that in models with strong BH feedback (IMBH6 per cent + PL1, IMBH6 per cent + MC01, and BVR06 + MC01) the transition from $f_{\rm ret} \sim 0$ to $f_{\rm ret} \sim 0.8$ is not as sharp as in the other cases we consider (remarkably, such difference is not present in the temperature plots of Fig. 13). In such models, haloes with masses in the range $M_{\rm crit} \leqslant M_{\rm halo} \lesssim 5\, M_{\rm crit}$ are relatively poor in gas, despite being able to form luminous objects at their centre. Such a luminous but gas-poor halo population starts developing at $z \sim 12$, and becomes increasingly important when lower redshifts are considered: for instance, at $z \sim 8$ this population is present also in models with intermediate BH feedback, and can span a factor of ∼10 in mass. If such objects actually exist and survive until present, they should be characterized by a high *M*/*L* ratio, a low gas content, and a mass $\sim 10^8\,{\rm M}_\odot$. Such properties remind us of the dwarf spheroidal galaxies of the Local Group (see Mateo 1998), although it might just be a coincidence. Further investigation is needed to address this issue.

5 DISCUSSION

5.1 Do neutral regions exist below redshift 11?

The three-year *WMAP* results (Spergel et al. 2007) for the electron scattering optical depth can be interpreted as indicating a sudden

[14] In most of the regimes, we are considering, the cooling rate is due to H_2 molecules. An increase in density results in both an increase in the cooling rate per molecule (which is $\propto \rho$) and an increase in the abundance of molecules.

reionization at $z \simeq 11$. In such a scenario, neutral regions essentially cease to exist as soon as reionization happens, and the effects of BHs at $z \lesssim 11$ would become negligible.

(i) The 21-cm brightness temperature differences would be severely quenched because of the lack of neutral H ($\delta T_{\rm B}$ is proportional to the density of neutral H atoms). Even if it were not, it is reasonable to expect that the reionization takes the IGM temperature $T_{\rm k}$ to $\sim 10^4$ K, and the BH heating would be unable to drastically change $T_{\rm k}$; the changes in $T_{\rm spin}$ would be even smaller.

(ii) The high IGM temperature we just mentioned would probably have important effects on structure formation, but that is a feedback effect from *stellar* sources, rather than from BHs.

In short, the effects of BHs can be clearly observed only at redshifts before the end of reionization process. In the case of a sudden reionization at $z \simeq 11$, they would become extremely difficult to detect, except perhaps in our models with the strongest BH feedback.

However, the sudden reionization scenario appears unrealistic. In fact, practically all the theoretical models predict that the reionization process is quite extended in time. In particular, the most recent numerical simulations (e.g. Iliev et al. 2007; Mesinger & Furlanetto 2007; Santos et al. 2007; Zahn et al. 2007) essentially agree in the prediction that the end of the overlap phase (i.e. the time when the volume filling factor of neutral regions becomes negligible) is at redshift $6.5 \lesssim z_{\rm overlap} \lesssim 8$. Fig. 3 of Santos et al. 2007 is particularly useful for our purposes, since it includes not only the evolution of the volume-averaged ionization fraction (solid line), but also a similar curve where complete ionization is assumed within the ionized 'bubbles' (dashed line): it is quite reasonable to expect the volume filling-factor of neutral regions to drop below $\sim$0.1 when such curve exceeds 0.8–0.9, that is, at $z \lesssim 7$–8.

Such behaviour is broadly consistent also with analytical models such as the one presented in (Choudhury & Ferrara 2006) (in their fig. 1(a) the volume-averaged neutral fraction goes below 0.1 already at $z \simeq 9$, but declines below 0.01 only at $z \lesssim 6$). It is also important to point out that such low values for $z_{\rm overlap}$ are usually obtained in models based on the three-year *WMAP* data, whereas models based upon one-year *WMAP* data (Kogut et al. 2003; Spergel et al. 2003) lead to significantly higher values of $z_{\rm overlap}$ (for instance, see Iliev et al. 2007, which presents the results of simulations based on both sets of parameters).

Furthermore, observations of the Gunn–Peterson troughs in the spectra of quasars at $z \gtrsim 6$ (see e.g. Fan et al. 2002, 2006b), and measurements of the evolution of the density of bright Lyman α emitters at $5.7 \lesssim z \lesssim 7$ (Kashikawa et al. 2006; Iye et al. 2006; Ota et al. 2007) might hint that we are actually observing the final stages of overlap; but the interpretation of the data is difficult and the issue is still under intense debate (see e.g. Malhotra & Rhoads 2004; Fan, Carilli & Keating 2006a; Mesinger & Haiman 2007; Dijkstra, Wyithe & Haiman 2007).

In short, it seems reasonably likely that the volume filling factor of neutral regions remained significant ($\gtrsim 0.1$) at least until redshift 7–8, and maybe even at lower redshifts; nonetheless, it is also possible (e.g. if the three-year *WMAP* results are underestimating $\tau_{\rm e}$) that a dearth of neutral regions at $z \lesssim 10$ will prevent the detection of the effects we discuss.

5.2 Comparison with previous works about BH feedback

Our analysis of feedback effects from high-redshift BHs has many links with the former study by RO04 (and also with Ricotti et al. 2005). However, there are some crucial differences between the assumptions in the two sets of models, which lead to important differences in the results.

(i) The most important difference is likely to be in the growth histories of the BH densities. All of the RO04 models reach $\rho_{\rm BH} \gtrsim 10^5$ M$_\odot$ Mpc^{-3} (in their notation, $\omega_{\rm BH} \sim 1.7 \times 10^{-5}$; cf. the lower panel of their fig. 2) at redshifts $\geqslant 15$, whereas at $z = 15$ none of our models exceeds $\rho_{\rm BH} = 10^3$ M$_\odot$ Mpc^{-3}. This difference becomes less important when going to lower redshifts. The IMBH-6 per cent growth history actually overtakes the RO04 predictions at $z \lesssim 6 - 7$. But all the other growth histories we consider are at most comparable to the RO04 models even at $z = 5$.

(ii) We assume a constant duty cycle ($y = 0.03$, 0.06 or 0.10, depending on the model), whereas in the RO04 models this quantity strongly depends on redshift (see the bottom panel of their fig. 3): it is assumed to be 1 at high redshifts ($z \geqslant 14$, $z \geqslant 19$ or $z \geqslant 24$), but rapidly falls to 10^{-3} when lower redshifts are considered ($z \leqslant 13$ or $z \leqslant 8$).

(iii) RO04 restrict their analysis to an intrinsically absorbed Sazonov et al. (2004) spectrum; their treatment of radiation transfer is more detailed than in the present paper, but as they are not limiting themselves to the neutral-IGM, their background spectrum is likely to extend to lower energies than ours, resembling the thin solid line in Fig. 1.

(iv) The RO04 models include also a stellar contribution.

Because of all these differences, the RO04 models predict a much larger energy injection into the IGM (at $z \gtrsim 15$ the difference can easily amount to a factor of $\gtrsim 10^3$). At lower redshifts ($z \lesssim 8$–9) such difference is erased (or even reverted), mostly because of the reduction in the RO04 duty cycle.

Taking into account these differences, the results of this paper are reasonably consistent with those of RO04. In fig. 5 of RO04, the ionized fraction and the IGM temperature are shown for different models. Complete ionization is achieved already at $z \sim 7$–8, while in our models $x_{\rm HI}$ is always less than 1 at $z > 6$ (but in most of our models complete reionization is never reached). This difference is simply explained by the presence of a stellar component in the RO04 semi-analytical model. For the same reason, IGM temperatures of 10^4 K are reached at $z \sim 8$–10 in our paper and at $z \sim 20$–25 in RO04. The Thomson optical depth derived by RO04 is $0.1 \lesssim \tau_{\rm e} \lesssim 0.2$, but a fraction $\tau_{\rm e} \sim 0.06$ is due to stars. Thus, the contribution of BHs to the Thomson optical depth in RO04 models is $\tau_{\rm e} \approx 0.04$–0.14, which is consistent with our findings ($\tau_{\rm e} \lesssim 0.07$). Furthermore, RO04 aim to reproduce the Thomson optical depth derived from one-year *WMAP* results ($\tau_{\rm e} \simeq 0.17 \pm 0.05$), which is considerably higher than in the three-year *WMAP* measurements ($\tau_{\rm e} \simeq 0.09 \pm 0.03$).

Ricotti et al. (2005) also study the effects on the 21-cm line; but, in their fig. 10, $\delta T_{\rm b}$ starts increasing already at $z \sim 20$–25, because of the strong increase in the IGM temperature due to the BH emission. The predicted peak in $\delta T_{\rm B}$ is of the order of only a few mK, a factor of $\sim$10 smaller than in our models. The low ($\lesssim$0.2) neutral fraction in their models is the likely cause of this discrepancy, as it implies a low τ_{21} in equation (25).

5.3 Other X-ray feedback mechanisms

Observations of local star-burst galaxies (Grimm, Gilfanov & Sunyaev 2003; Ranalli, Comastri & Setti 2003; Gilfanov, Grimm & Sunyaev 2004) find a correlation between star formation and X-ray luminosity. As was noted in Glover & Brand (2003), Furlanetto (2006), Pritchard & Furlanetto (2007) and Santos et al. (2007), it is reasonable to expect that also high-redshift star formation is

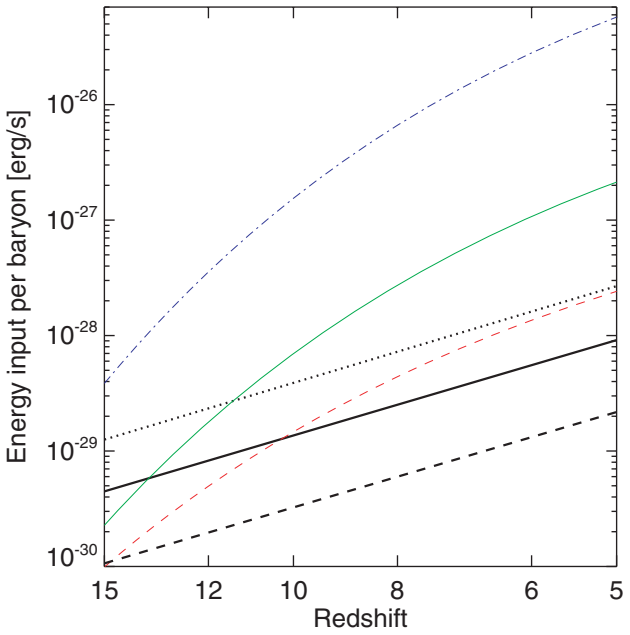

Figure 14. Redshift evolution of the total energy input per baryon due to the background produced by X-ray emission associated with star formation (thick lines; the two lines refer to power-law SEDs with different photon index: $\Gamma = 1.5$ for the dashed line, $\Gamma = 2.0$ for the solid line, and $\Gamma = 2.5$ for the dotted line), assuming $f_{\rm X} = 1$. For comparison, we show also the energy input in models where BH emission was considered (IMBH-6 per cent + MC01: thin dot–dashed line; IMBH-3 per cent + PL1: thin solid line; BVR06 + SOS1: thin dashed line).

associated with X-ray emission, although an unknown (and possibly important) correction factor $f_{\rm X}$ should be introduced to quantify the differences between the local and the primordial environment.

The effects of such emission (and whether they can be distinguished from the ones presented in this paper) will be thoroughly investigated in a companion paper (Ripamonti, Nusser & Zaroubi, in preparation). Here, we just compare the energy input due to BHs with the one due to X-ray emission associated with star formation. This was done by assuming that the SED of such emission is a power law with photon index in the $1.5 \leqslant \Gamma \leqslant 2.5$ range, and that the star formation rate is similar to the one shown in fig. 1b of Choudhury & Ferrara (2006). In Fig. 14, we show that in the lower redshift range we consider ($z \lesssim 10$) the expected energy input is only a fraction of the BH contribution of most of our models, and is comparable only to the BH model with the weakest feedback; at higher redshifts the star formation associated X-ray emission might be more important or even dominant, but the overall energy input is small.

In short, if the unknown factor $f_{\rm X}$ is not much larger than 1, the effects of the X-ray emission associated with star formation should be at most comparable to the ones of the weakest of our BH models (such as the BVR06 + SOS1 case).

6 SUMMARY AND CONCLUSIONS

We have examined how a population of accreting BHs might affect the pre-reionization Universe, looking in particular at the effects upon the neutral regions outside the first ionized 'bubbles', where stellar feedback is likely small. We explored a number of scenarios for the growth of the cosmological BH density, and considered several possible SEDs. Both of these components are in broad agreement with observational constraints (e.g. the results about the X-ray background by Dijkstra et al. 2004).

Our analysis started from how the energy input from the diffuse radiation due to the BH population might affect the temperature and ionization level of the IGM far away from ionized regions where local effects are important. Given the Dijkstra et al. (2004) constraints, it is not surprising that BH emission in our models leads only to partial ionization: the main effect of BH emission is then the increase in the temperature of the IGM, which easily reaches levels $\gtrsim 10^3$ K in all the cases we have considered.

We then explored a number of possible indirect consequences of the energy input.

(i) CMB measurements appear unable to constrain any of our models, since all of them comfortably fit observational constraints from *WMAP*.

(ii) 21-cm observations appear extremely promising, since in most of the BH models the predicted $\delta T_{\rm b}$ should be easily detectable with the next generation of 21-cm experiments (e.g. LOFAR), especially if stellar Lyman α, coupling is really present.

(iii) The critical mass for haloes to be able to cool, collapse and form stars is significantly enhanced at $z \lesssim 10$ and in some of our models it becomes $\sim$100 times larger than in the unperturbed case. This allows star formation only in haloes with virial temperatures $\gtrsim 10^4$ K, that is, prevents (or, in models with weak feedback, significantly reduces) the formation of Population III objects for $z \lesssim 9$.

(iv) Gas depletion might occur in the models with intermediate-to-strong BH feedback, and for relatively low virialization redshifts: haloes with masses between $M_{\rm crit}$ and 3–10$M_{\rm crit}$ appear to be able to form stars at their centre, but their baryonic fraction is considerably lower than the cosmological average.

The most relevant of our results appears to be the one about 21-cm observations, since it might be falsified (or confirmed) by forthcoming observations. To our knowledge, the only mechanism which should be able to heat the IGM outside ionized regions in a comparable way is the X-ray emission associated with star formation, as was proposed by Glover & Brand (2003), Furlanetto (2006) and Pritchard & Furlanetto (2007). We leave the detailed comparison between the two models to a future paper (Ripamonti et al., in preparation), where we will also investigate whether it is possible to distinguish between the two scenarios, e.g. by using the spatial power spectrum.

We stress that most of our conclusions strongly depend on the details of the reionization process, and in particular on the survival of neutral regions down to redshift $\sim$7–8. Recent simulations (e.g. Santos et al. 2007) and observations (e.g. Fan et al. 2002; Kashikawa et al. 2006) hint that the overlapping phase lasted for a long time and suggest the existence of patches with a significant neutral fraction even at $z \lesssim 7$. However, the scenario of an earlier reionization cannot be rejected at present: in such a case, BH signatures (such as the effects on the properties of 21-cm radiation) become difficult or impossible to detect. On the other hand, if the predictions of simulations are correct, the effects of BH emission might enhance the 21-cm contrast between neutral and ionized patches, improving our capability of studying the $z \sim 7$–12 Universe, and providing important information on the duration and the end of the reionization phase.

ACKNOWLEDGMENTS

We thank R. Salvaterra for clarifications about the CS07 results, F. Haardt, G. Mellema, R. Thomas and M. Volonteri for useful

discussions, and the anonymous referee for several suggestions about improving the manuscript. We also thank K. Visser for assistance in working with the HPC cluster of the Centre for High Performance Computing and Visualization of the University of Groningen, where most of our computations were carried out. ER and MM thank the Institute for Theoretical Physics of the University of Zürich, and the Kapteyn Astronomical Institute of the University of Groningen for the hospitality during the preparation of this paper. ER acknowledges support from the Netherlands Organization for Scientific Research (NWO) under project number 436016, and MM acknowledges support from the Swiss National Science Foundation, project number 200020-109581/1 (Computational Cosmology & Astrophysics). SZ is a member of the LOFAR project which is partially funded by the European Union, European Regional Development Fund, and by 'Samenwerkingsverband Noord-Nederland', EZ/KOMPAS.

REFERENCES

Abel T., Anninos P., Zhang Y., Norman M. L., 1997, New Astron., 2, 181
Allison A. C., Dalgarno A., 1969, ApJ, 158, 423
Anninos P., Zhang Y., Abel T., Norman M. L., 1997, New Astron., 2, 209
Bauer F. E., Alexander D. M., Brandt W. N., Schneider D. P., Treister E., Hornschemeier A. E., Garmire G. P., 2004, AJ, 128, 2048 (B04)
Becker R. H. et al., 2001, AJ, 122, 2850
Begelman M. C., Volonteri M., Rees M. J., 2006, MNRAS, 370, 289 (BVR06)
Bromm V., Loeb A., 2003, ApJ, 596, 34
de Bruyn A. G., Zaroubi S., Koopmans L. V. E., 2007, The LOFAR Epoch of Reionization Project Plan. Available from http://www.astro.rug.nl/LofarEoR
Chen X., Kamionkowski M., 2004, Phys. Rev. D, 70d, 3502
Choudhury T. R., Ferrara A., 2006, MNRAS, 371, L55
Ciardi B., Madau P., 2003, ApJ, 596, 1
Ciardi B., Salvaterra R., 2007, MNRAS, 381, 1137 (CS07)
Crain R. A., Eke V. R., Frenk C. S., Jenkins A., McCarthy I. G., Navarro J. F., Pearce F. R., 2007, MNRAS, 377, 41
De Luca A., Molendi S., 2004, A&A, 419, 837
Dijkstra M., Haiman Z., Loeb A., 2004, ApJ, 613, 646
Dijkstra M., Wyithe J. S. B., Haiman Z., 2007, MNRAS, 379, 253
Djorgovski S. G., Castro S., Stern D., Mahabal A. A., 2001, ApJ, 560, L5
Eisenstein D. J., Loeb A., 1995, ApJ, 443, 11
Fan X. et al., 2001, AJ, 122, 2833
Fan X., Narayanan V. K., Strauss M. A., White R. L., Becker R. H., Pentericci L., Rix H.-W., 2002, AJ, 123, 1247
Fan X. et al., 2003, AJ, 125, 1649
Fan X., Carilli C. L., Keating B., 2006a, ARA&A, 44, 415
Fan X. et al., 2006b, AJ, 132, 117
Field G. B., 1958, Proc. Institute of Radio Engineers, 46, 240
Field G. B., 1959, ApJ, 129, 525
Furlanetto S. R., 2006, MNRAS, 371, 867
Galli D., Palla F., 1998, A&A, 335, 403
Gilfanov M., Grimm H.-J., Sunyaev R., 2004, MNRAS, 347, L57
Glover S. C. O., Brand P. W. J. L., 2003, MNRAS, 340, 210
Grimm H.-J., Gilfanov M., Sunyaev R., 2003, MNRAS, 339, 793
Haardt F., Madau P., 1996, ApJ, 461, 20
Haehnelt M. G., Rees M. J., 1993, MNRAS, 263, 168
Heger A., Woosley S. E., 2002, ApJ, 567, 532
Hickox R. C., Markevitch M., 2007, ApJ, 661, L117 (HM07)
Iliev I. T., Mellema G., Shapiro P. R., Pen U.-L., 2007, MNRAS, 376, 534
Islam R. R., Taylor J. E., Silk J., 2003, MNRAS, 340, 647
Islam R. R., Taylor J. E., Silk J., 2004, MNRAS, 354, 427
Iye M. et al., 2006, Nat, 443, 186
Kashikawa N. et al., 2006, ApJ, 648, 7
Kogut A. et al., 2003, ApJS, 148, 161
Koushiappas S. M., Bullock J. S., Dekel A., 2004, MNRAS, 354, 292
Kuhlen M., Madau P., Montgomery R., 2006, ApJ, 637, L1
Lodato G., Natarajan P., 2006, MNRAS, 371, 1813
Lodato G., Natarajan P., 2007, MNRAS, 377L, 64
Loeb A., Rasio F. A., 1994, ApJ, 432, 52
Machacek M. E., Bryan G. L., Abel T., 2003, MNRAS, 228, 273
Madau P., Rees M. J., Volonteri M., Haardt F., Oh S. P., 2004, ApJ, 604, 484
Malhotra S., Rhoads J. E., 2004, ApJ, 617, L5
Mateo M. L., 1998, ARAA, 36, 435
Mesinger A., Furlanetto S. R., 2007, ApJ, 669, 663
Mesinger A., Haiman Z., 2007, ApJ, 660, 923
Moretti A., Campana S., Lazzati D., Tagliaferri G., 2003, ApJ, 588, 696
Nusser A., 2005, MNRAS, 359, 183
Osterbrock D. E., 1989, Astrophysics of Gaseous Nebulae and Active Galactic Nuclei. University Science Books, Sausalito, CA (USA)
Ota K. et al., 2007, preprint (arXiv:0707.1561)
Pelupessy F. I., Di Matteo T., Ciardi B., 2007, ApJ, 665, 107
Pengelly R. M., 1964, MNRAS, 127, 145
Pritchard J. R., Furlanetto S. R., 2007, MNRAS, 376, 1680
Ranalli P., Comastri A., Setti G., 2003, A&A, 399, 39
Ricotti M., Ostriker J. P., 2004, MNRAS, 352, 547 (RO04)
Ricotti M., Ostriker J. P., Gnedin N. Y., 2005, MNRAS, 357, 207
Ripamonti E., 2007, MNRAS, 376, 709 (R07)
Ripamonti E., Haardt F., Ferrara A., Colpi M., 2002, MNRAS, 334, 401
Ripamonti E., Mapelli M., Ferrara A., 2007, MNRAS, 375, 1399 (RMF07)
Salvaterra R., Haardt F., Ferrara A., 2005, MNRAS, 362L, 50
Salvaterra R., Haardt F., Volonteri M., 2007, MNRAS, 374, 761
Santos M. G., Amblard A., Pritchard J., Trac H., Cen R., Cooray A., 2007, preprint (arXiv:0708.2424)
Sazonov S. Y., Ostriker J. P., Sunyaev R. A., 2004, MNRAS, 347, 144
Seljak U., Zaldarriaga M., 1996, ApJ, 469, 437
Seljak U., Sugiyama N., White M., Zaldarriaga M., 2003, Phys. Rev. D, 68h, 3507
Shakura N. I., Sunyaev R. A., 1973, A&A, 24, 337
Shlosman I., Frank J., Begelman M. C., 1989, in Osterbrock D. E., Miller J. S., eds, Proc. IAU Symp. 134, Active Galactic Nuclei. Kluwer Academic Publishers, Dordrecht, p. 462
Shlosman I., Frank J., Begelman M. C., 1990, Nat, 345, 679
Shull J. M., van Steenberg M. E., 1985, ApJ, 298, 268
Smith F. J., 1966, P&SS, 14, 929
Spergel D. N. et al., 2003, ApJS, 148, 175
Spergel D. N. et al., 2007, ApJS, 170, 377
Steidel C. C., Hunt M. P., Shapley A. E., Adelberger K. L., Pettini M., Dickinson M., Giavalisco M., 2002, ApJ, 576, 653
Tegmark M., Silk J., Rees M. J., Blanchard A., Abel T., Palla F., 1997, ApJ, 474, 1
Thomas R. M., Zaroubi S., 2008, MNRAS, 384, 1050
Toomre A., 1964, ApJ, 139, 1217
Umemura M., Loeb A., Turner E. L., 1993, ApJ, 419, 459
Valdès M., Ferrara A., Mapelli M., Ripamonti E., 2007, MNRAS, 377, 245
Volonteri M., Perna R., 2005, MNRAS, 358, 913
Volonteri M., Rees M. J., 2005, ApJ, 633, 624
Volonteri M., Rees M. J., 2006, ApJ, 650, 669
Volonteri M., Haardt F., Madau P., 2002, Ap&SS, 281, 501
Volonteri M., Haardt F., Madau P., 2003, ApJ, 582, 559
Volonteri M., Salvaterra R., Haardt F., 2006, MNRAS, 373, 121
White R. L., Becker R. H., Fan X., Strauss M. A., 2003, AJ, 126, 1
Wild J. P., 1952, ApJ, 115, 206
Zahn O., Lidz A., McQuinn M., Dutta S., Hernquist L., Zaldarriaga M., Furlanetto S. R., 2007, ApJ, 654, 12
Zaroubi S., Thomas R. M., Sugiyama N., Silk J., 2007, MNRAS, 375, 1269 (Z07+)
Zdziarski A. A., Svensson R., 1989, ApJ, 344, 551
Zygelman B., 2005, ApJ, 622, 1356

This paper has been typeset from a TEX/LATEX file prepared by the author.